

UNCLASSIFIED

AD NUMBER

AD204392

LIMITATION CHANGES

TO:

Approved for public release; distribution is unlimited.

FROM:

Distribution authorized to DoD and DoD contractors only; Administrative/Operational Use; NOV 1958. Other requests shall be referred to Arnold Engineering Development Center, Arnold AFB, TN.

AUTHORITY

AEDC ltr, 9 Sep 1994

THIS PAGE IS UNCLASSIFIED



AEDC-TR-58-20  
ASTIA DOCUMENT NO.:  
AD-204392

**ARCHIVE COPY  
DO NOT LOAN**

**EXPERIMENTAL INVESTIGATION  
OF THE HEMISPHERE-CYLINDER AT  
HYPERVELOCITIES IN AIR**

By

**J. Christopher Boison  
GDF, ARO, Inc.**

**November 1958**

PROPERTY OF U. S. AIR FORCE  
AEDC LIBRARY  
AF 40(600)-100 SUP. 6 (1-1)

Approved for public release; distribution unlimited.

*per letter  
dated 9/9/94*

**ARNOLD ENGINEERING  
DEVELOPMENT CENTER**

**AIR RESEARCH AND DEVELOPMENT COMMAND**



AEDC TECHNICAL LIBRARY



5 0720 00030 9320

*Additional copies* of this report may be obtained from

ARMED SERVICES TECHNICAL INFORMATION AGENCY  
ARLINGTON HALL STATION  
ARLINGTON 12, VIRGINIA

ATTN: TISVV

note

Department of Defense contractors must be established for ASTIA services, or have their need-to-know certified by the cognizant military agency of their project or contract.



DEPARTMENT OF THE AIR FORCE  
HEADQUARTERS ARNOLD ENGINEERING DEVELOPMENT CENTER (AFMCI)  
ARNOLD AIR FORCE BASE, TENNESSEE


9 Sep 94

MEMORANDUM FOR DTIC/FDAC  
Cameron Station  
Alexandria VA 22405-6145

FROM: AEDC/DO  
1099 Avenue C  
Arnold AFB TN 37389-9010

SUBJECT: Distribution Statement Change for AEDC-TR-58-20 (AD204392)

1. Subject report has been reviewed by the AF OPR. It was determined that the report can now be marked, "Cleared for Public Release - Distribution Unlimited."
2. This change is effective immediately. Please contact the undersigned at (615)-454-7813/DSN 340-7813 if there are any questions.

  
BOBBIE JONES  
STINFO Officer  
Directorate of Test Operations

cc: AEDC Tech Files  
AEDC Tech Publications

EXPERIMENTAL INVESTIGATION  
OF THE HEMISPHERE-CYLINDER  
AT HYPERVELOCITIES IN AIR

By

J. Christopher Boison  
GDF, ARO, Inc.

November 1958

ARO Project No. 361703

Contract No. AF 40(600)-700 S/A 13(59-1)

## CONTENTS

	<u>Page</u>
ABSTRACT . . . . .	5
NOMENCLATURE . . . . .	5
INTRODUCTION . . . . .	7
APPARATUS. . . . .	8
Wind Tunnel . . . . .	8
Models . . . . .	9
Instrumentation . . . . .	9
PROCEDURE. . . . .	13
PRECISION . . . . .	14
RESULTS AND DISCUSSION.. . . .	16
Pressure . . . . .	16
Heat Transfer . . . . .	19
Drag . . . . .	20
Shock Detachment. . . . .	21
CONCLUSIONS . . . . .	24
REFERENCES . . . . .	25
APPENDIX A . . . . .	29

## TABLE

1. Summary of Qualitative Analysis of Relaxation Phenomena in Stagnation Region of Hemisphere-Cylinder Models Tested in Hotshot I . . . . .	30
---	----

## ILLUSTRATIONS

Figure

1. Hotshot I Schematic. . . . .	31
2. Typical Raw Data - Pressure . . . . .	32
3. Hemisphere-Cylinder Model Dimensions . . . . .	33
4. Hemisphere-Cylinder Drag Model (Schematic). . . . .	34
5. Schematic of Data Recording System . . . . .	35
6. Typical Raw Data - Drag . . . . .	36
7. Hemisphere-Cylinder Pressure Transducer Installation . . . . .	37
8. Typical Raw Data - Heat Transfer . . . . .	38

<u>Figure</u>	<u>Page</u>
9. Hemisphere-Cylinder Heat Transfer Model . . . . .	39
10. Hemisphere-Cylinder Heat Transfer Gage Installation .	40
11. Hemisphere-Cylinder Drag Model (Photo). . . . .	41
12. Schlieren Photograph of Hemisphere-Cylinder. . . . .	42
13. Luminosity Photograph of Hemisphere-Cylinder . . . . .	42
14. Reynolds Number per Foot - Mach Number Range . . .	43
15. Density Altitude - Velocity Comparison. . . . .	44
16. Hemisphere-Cylinder Pressure Distribution, Comparison of Theory and Experiment . . . . .	45
17. Comparison of Pressure Distribution with Theory for a Hemisphere-Cylinder in Hotshot I . . . . .	46
18. Local Relaxation Characteristic Time Ratio for 2-inch Radius Hemisphere in Hotshot I . . . . .	47
19. Comparison of Pressure Distribution with Theory for a Hemisphere-Cylinder in Hotshot I . . . . .	48
20. Hemisphere-Cylinder Heat Transfer Distribution, Comparison of Theory and Experiment . . . . .	49
21. Average Experimental Pressure Distribution Used for Heat Transfer Distribution Calculations for $M_\infty > 10$ . . .	50
22. Comparison of Heat Transfer Distribution with Theory for a Hemisphere-Cylinder in Hotshot I. . . . .	51
23. Stagnation Point Heat Transfer for a Hemisphere-Cylinder in Hotshot I . . . . .	52
24. Effect of $\rho\mu$ Variation across Stagnation Point Boundary Layer. . . . .	53
25. Drag Coefficient for a Hemisphere-Cylinder, Comparison of Theory and Experiment. . . . .	54
26. Comparison of Shock Detachment Distance with Theory and Experiment . . . . .	55

## ABSTRACT

Pressure, heat transfer, drag, and shock detachment data were obtained for a hemisphere-cylinder model in the GDF Hotshot I hypervelocity wind tunnel. Data were obtained for zero angle of incidence at Mach numbers from 11 to 18 and free-stream Reynolds numbers per foot from  $25 \times 10^3$  to  $270 \times 10^3$ . Stagnation enthalpies and reservoir temperatures ranged from  $5.7 \times 10^7$  to  $15.6 \times 10^7$  ft<sup>2</sup>/sec<sup>2</sup> and 4000 to 8000°K, respectively.

The data indicate that pressure distribution, heat transfer distribution, and drag coefficient were independent of the range of variables investigated. Modified Newtonian, Matched Prandtl-Meyer theory for  $\gamma = 1.4$  was found to predict the hemispherical pressure distribution quite accurately. When real gas thermal equilibrium was assumed, Lees' heat transfer distribution theory in conjunction with the experimental pressure distribution was found to overestimate the heat transfer rates. When "frozen flow" around the body was assumed, better correlation with theory was obtained.

Pressure, heat transfer, and shock detachment measurements indicated the possibility of thermal non-equilibrium flow about the body and in the stagnation region. Although scatter of the stagnation point heat transfer data did not permit any quantitative conclusions when compared to the Lees and Fay-Riddell theories, a general agreement in trend was noted.

## NOMENCLATURE

A	Body frontal area
$C_D$	Drag coefficient, $\text{drag}/q_\infty A$
$C_{p_{\max}}$	Stagnation point pressure coefficient, $\frac{P_s - P_\infty}{q_\infty}$
$c_p$	Specific heat at constant pressure
D	Body diameter
$D_i$	Diffusion coefficient
E	Specific internal energy
H	Total specific enthalpy
h	Static specific enthalpy
k	Thermal conductivity

L	Lewis number, $D_i \rho c_p / k$
M	Mach number
$Nu_w$	Nusselt number, $\dot{q}_s \bar{c}_{p_w} / k_w (h_s - h_w)$
P	Total pressure
p	Static pressure
q	Dynamic pressure, $\frac{1}{2} \rho u^2$
$\dot{q}$	Heat transfer rate
$R_N$	Body nose radius
$Re_e$	Reynolds number based on properties at edge of boundary layer, $\rho_e u_e s / \mu_e$
$Re_w$	Reynolds number based on properties at body surface, $\rho_w u_e s / \mu_w$
s	Surface distance from body stagnation point
T	Temperature
$T_{o_{nom}}$	Reservoir temperature defining nominal "standard shot" condition (see Procedure section of report)
t	Time
u	Flow velocity
v	Volume
$Z_\rho$	Density altitude
$\gamma$	Ratio of specific heats
$\delta$	Shock detachment distance
$\delta^*$	Boundary layer displacement thickness
$\theta$	Angle between normal to body and axis of symmetry
$\mu$	Absolute viscosity
$\rho$	Density
$\rho_{sl}$	Reference density, $2.5 \times 10^3$ slugs/ft <sup>3</sup>
$\tau$	Relaxation time

#### SUBSCRIPTS

e	Local external flow conditions
o	Reservoir condition
s	Body stagnation point
sh	Across bow shock
w	Local conditions at body surface
$\infty$	Free-stream conditions ahead of bow shock

## INTRODUCTION

During the past few years, a considerable number of theoretical and experimental studies have been made to determine the aerodynamic and heat transfer characteristics of blunt-nose bodies. Part of this effort has been expended to obtain more reliable information in the hypervelocity regime regarding the aerodynamic and chemical behavior of air passing over these bodies and the subsequent high heat transfer rates. The analysis of these problems for hypervelocity flows is complex; adding to the complexity are such phenomena as real gas effects, viscous interactions, and low density effects, to mention a few, as well as the lack of fundamental data regarding the behavior of air at elevated temperatures and densities. These, along with others, can significantly alter, for example, the performance, stability, structural design, and payload of a hypersonic vehicle. It is known that a small savings in structural weight can magnify itself considerably in propulsion system weight reduction. Each investigator seeks to simulate as much of the actual flight behavior in his experiments as possible. The simulation of all the free-flight parameters simultaneously in one test, short of a full-scale test vehicle, is not attainable at the present time. However, it is possible to simulate various combinations of these parameters and then assess the effects of the nonsimulated conditions by theory or other experimental correlations. It is felt that the Hotshot type facility can contribute to the quest for data since it can simulate velocity (stagnation enthalpy), Mach number, and density in regions of interest.

Thus, the purpose of this investigation was to add to the accumulation of data at hypervelocity conditions. The specific study is related to the hemisphere-cylinder at zero angle of incidence with a highly cooled boundary layer.

The experimental investigation was conducted in tunnel Hotshot I, a hypervelocity wind tunnel in the Gas Dynamics Facility at Arnold Engineering Development Center (GDF-AEDC). The test was jointly sponsored by the Air Force Ballistic Missile Division and the Arnold Engineering Development Center, the Air Research Development Command, and was initially suggested and encouraged by the Ramo-Wooldridge Corporation.

Data on pressure and heat transfer distribution, drag, and shock detachment distance were obtained for a Mach number range from 11 to 18 and free-stream Reynolds numbers per foot from  $25 \times 10^3$  to  $270 \times 10^3$ . Stagnation enthalpies and reservoir temperatures ranged from  $5.7 \times 10^7$  to  $15.6 \times 10^7$  ft<sup>2</sup>/sec<sup>2</sup> and 4000 to 8000°K, respectively.

## APPARATUS

### WIND TUNNEL

The principle and operation of Hotshot I have been described in Refs. 1 and 2. The basic components of this hypervelocity facility (Fig. 1) are:

1. Power supply - one-million joule capacitor bank
2. Arc chamber - 21.7 in.<sup>3</sup> internal volume
3. Conical nozzle - 5° half-angle divergence
4. Test section - 16-in. diam
5. Vacuum chamber

Electrical energy stored in the capacitor bank is released in the arc chamber and through a constant-volume process produces a highly energized mass of air. The final thermodynamic state of the confined air is essentially controlled by the level of stored energy dissipated and by the initial density. A plastic diaphragm located slightly upstream of the throat is vaporized under the extreme conditions, thus initiating a quasi-steady expansion into the evacuated nozzle and vacuum tank sections.

For any given final thermodynamic state in the arc chamber, a reasonable latitude in flow Mach number may be achieved by varying the throat diameter. Because of the large heat-transfer rates and shear stresses in the vicinity of the throat, small replaceable tungsten throat inserts are required to withstand the extreme conditions.

Run times lasting from 25 to 50 msec are achieved depending upon reservoir conditions and expansion area ratio. Generally, valid test data may be obtained during the period between initiation of quasi-steady flow and return of the starting shock after its reflection from the end of the vacuum tank. However, the valid test data period may be prematurely shortened by the occurrence of an afterbody wake separation propagating upstream from the sting support region. This phenomenon is generally observed while the tunnel is being operated at large throat diameters and could be attributed to propagation of disturbances upstream through the subsonic portion of the relatively thick afterbody boundary layer. The separated region will almost always eventually engulf the complete model afterbody. The photograph in Fig. 2 (lower right) shows a typical example of the separated region.

Presently because of the relatively low densities prevailing in the test section, only laminar boundary layers can be expected to exist on the test models. Attempts to trip the boundary layer during previous tests had proved unsuccessful.

## MODELS

Three hemisphere-cylinder models were tested. The 4-in. -diam pressure and heat transfer models were geometrically identical. In order to allow "drawing" of the 2-in. drag model from its mold, a 2-deg flare was provided on the afterbody. Figures 3 and 4 give the more important dimensional details, including gage locations, for these models.

Both the pressure and heat transfer models were machined of 2204-T4 aluminum bar stock with a wall thickness of 0.2 in. and a length to diameter ratio of 1.5. The drag model, formed of resin impregnated fiberglass, had a wall thickness of 0.031 in. and a length to diameter ratio of 1.0.

It was not necessary to maintain highly polished surface finishes because transition to turbulent flow could not occur and because model surface erosion which resulted from impingement of minute throat and arc chamber particles could not be avoided.

## INSTRUMENTATION

Instrumentation techniques used in Hotshot I are somewhat unconventional because of the conditions under which the transducers have to operate. These transducers must be capable of millisecond time resolution, and a large signal output is required for effective operation in the field of intense noise produced during the arc discharge. The transducers used for measuring pressure and heat transfer on the model and the drag balance were designed and built at AEDC. Figure 5 shows the basic components of the data-recording system used with no modification for amplifying and recording the pressure, heat transfer, and drag transducer outputs. A detailed discussion of the data-recording system and of the various pressure transducers mentioned in the next section is given in Ref. 3.

### Pressure Measurement

Pressure transducers used in this experimental investigation may be categorized into three distinct groups: those for measuring pressures (1) in the arc chamber, (2) on the nozzle cone, and (3) on the model.

Two arc chamber pressures were measured simultaneously during each run. Early in the test program these pressures were measured with a variable-capacitance gage. Later one of these gages was exchanged for a strain-gage type transducer; both gages are available commercially. Calibration of the transducers was effected through the use of a 100,000-psi deadweight tester. The output of the variable-capacitance gage was recorded by photographing the signal as traced on an oscilloscope screen. The strain-gage transducer output was recorded on the 50-channel oscillograph, along with the outputs of the various transducers as discussed later. Typical arc chamber pressure records are shown in Fig. 6.

Low-impedance variable-reluctance transducers, also commercially available, were used to measure the static pressures along the nozzle cone. Because of the physical size of these transducers and limitations imposed on model size by tunnel "blockage" problems, it was not feasible to use these gages in the models since a moderate number was required to obtain a good pressure distribution. Therefore, a much smaller variable-reluctance transducer, developed at AEDC and known locally as the "Charliedyne", was used exclusively for model pressure measurement. Figure 7 shows a portion of the transducer installation in the model afterbody.

The "Charliedyne" is capable of resolving pressures probably below 50 microns of mercury. In fact, this lower limit is attributed to the noise level of the external instrumentation. Because this transducer has an exceedingly small internal volume, orifice diameters of 1/32 in. over a sizeable portion of the model forebody did not produce more than a millisecond rise time. Afterbody orifice diameters were increased to 1/16 in. to facilitate adequate time response to the inherently lower pressures in this region.

Since the "Charliedyne" operates as a differential-pressure gage, the reference sides were manifolded together to facilitate simultaneous calibration. During tunnel operation the reference sides were maintained at the initial tunnel pressure of two to three microns by using a ballast tank.

A typical analog record is shown in Fig. 2. The time-wise decrease in pressure (for example, orifice numbers 1, 2, 3, 20) is caused by the decay of reservoir conditions. This decay is caused by the depletion of mass in the arc chamber and by heat transfer to the arc chamber walls. Two self-luminosity photographs taken from the Fastax record of the run are included to show both an attached and separated flow on the afterbody. A reflection of the main bow shock from the rear observation window appears to be a second shock emanating from the upper portion of the forebody. This is caused by having to place the optical axis of the Fastax below the transverse axis of the tunnel to allow undisturbed schlieren observation. An obvious increase, approximately twofold, in afterbody pressure caused by flow separation can be seen in Fig. 2, orifice numbers 11 through 19.

Although the nozzle cone pressures may be used in determining the free-stream static pressure, only the model stagnation pressure was used to determine the conditions in the test section. Both methods are discussed in Ref. 2.

#### Heat Transfer Measurement

Nineteen gage locations on the heat transfer model were identical to those of the pressure model. The two remaining locations, model positions 19 and 20 (see Fig. 3), were reserved for pressure orifices. Position 19 was used to monitor the afterbody pressure-time history which readily indicated the occurrence of the previously mentioned flow separation. Stagnation point pressure was determined by applying an additive correction of three percent, based on Newtonian flow, to the pressure history of model position 20.

The Morgandyne, the heat gage used for this study, was designed and built at AEDC. This gage is unique in that it utilizes the variable-reluctance principle. A thin copper ring 0.010-in. thick, having an OD of 3/16 in. and ID of 1/16 in., is inductively coupled to an inner coil which is excited by a 20-kc carrier wave. Since the copper will change its resistance with a rise in temperature, this change produces a signal proportional to the total heat added to the copper. Thus, the gage under dynamic conditions in the tunnel acts as a calorimeter.\* Losses through the back side of the gage are minimized by a thick air film between the ring and inner portions of the gage. Quality control of the ring installation is essential for maintaining an adequate air film behind the copper sensing element. The copper ring is mounted flush and contoured to the model surface; thus, the creation of any significant disturbances in the laminar boundary layer is minimized. Laminar separation or shocks at the gage edges are considered to be more detrimental, in this instance, since local tripping of the boundary layer seems quite unlikely because of the small local Reynolds numbers. Measurement of surface profiles across the gage sensing elements indicates discontinuities generally less than 0.0005 in. relative to the model mean surface.

A distinct advantage of this gage is the relatively small sensing area, 3/16-in. diam, which for the present study obviated any geometric correction. The change in local aerodynamic parameters with surface distance is considered to be small compared to the hemispherical characteristic length of two inches. The stagnation point would be affected most with a tendency to produce a slightly lower absolute reading. This error is approximately equivalent to the change in heat transfer over the surface subtended by a one-deg solid angle.

---

\*See Ref. 4 for an excellent analysis of the calorimeter gage principle.

These possible heat transfer measurement errors are overshadowed by two other sources of error. Calibration techniques at the present time do not allow the dynamic simulation of the heat transfer history occurring during tunnel operation, and the decay of reservoir pressure during a run introduces a source of error which involves the accurate calculation of test section conditions as a function of run time. These problems are discussed later under Precision.

Figure 8 is a typical heat transfer oscillogram. The slight non-linearity of the heat gage output with time is caused by the decay in reservoir conditions. A larger throat diameter increases the non-linearity of the gage output with time because of the increased decay of reservoir conditions. Figures 9 and 10 show the external and internal gage installations, respectively.

#### Drag Measurement

One-component axial force measurements were made with an internal strain-gage balance, also developed at AEDC. This balance is viscously damped to about 40 percent of critical damping. Since a frequency response of approximately one kilocycle per second was deemed necessary to achieve a one millisecond rise time, it was necessary that the model be light; fiberglass construction fulfilled this requirement. However, to reduce interactions between the model, balance, and sting support, the balance and sting support were made as stiff as possible.

A typical drag oscillogram is presented in Fig. 6 and installation of the drag balance in Fig. 11.

#### Shock Detachment Measurement

Shock detachments were obtained by enlarging the schlieren negatives 15 times on a Comparator Microphotometer. Detachment distance as measured is the axial distance along the model centerline from the upstream side of the shock to the model stagnation point.

#### Optical Techniques

Schlieren, Fastax motion pictures, and an open-shutter still camera were used during this investigation.

The schlieren system used was the single-pass "Z" type which utilized a one-microsecond exposure time produced by a very intense spark source (approximately 3-msec exposure time) in conjunction with a Faraday magneto-optical shutter. Figure 12 is a typical schlieren photograph from which shock detachment or bow-shock shape data may be obtained.

The intense self-illumination produced by the air in the shock layer made it possible to take Fastax motion pictures during the complete run. A framing rate of approximately 4000 frames per second was generally used. This visual flow time-history produced qualitative information which was correlated with other physical measurements. It was especially beneficial in providing a second source for detecting the premature onset of flow separation about the body.

The open-shutter still camera produced a time-integrated image of the luminous field. Figure 13 is a typical photograph taken with this camera; again note the reflected bow-shock image caused by the off-axis photography.

### PROCEDURE

Because of the present operating characteristics of the Hotshot type facility, it is more efficient to conduct each type of basic test without interruption, and the data were taken in the following chronological order:

1. Pressure distribution
2. Heat transfer distribution
3. Axial force

Schlieren, Fastax, and open-shutter photographs were taken during all phases.

The goal of the test was to obtain data for each of the three phases under the same conditions and to cover as reasonable a range of free-stream Mach number as possible for three nominal stagnation temperatures: 4000, 6000, and 8000°K. The latter temperatures and the information tabulated here form the three "standard shots" of this investigation.

$T_{o_{nom}}, ^\circ K$	4000	6000	8000
$\rho_o / \rho_{sl}$	70	49.12	35
$P_o, \text{ psi}$	14,950	17,000	18,030
$H_o, \text{ ft}^2 / \text{sec}^2$	$5.73 \times 10^7$	$10.1 \times 10^7$	$15.55 \times 10^7$

These "standard shots" were selected to avoid the long and tedious calculations required to determine a complete isentropic expansion for a real gas from the arc chamber to the test section for the infinite number of combinations available. Since it is not possible to reproduce exactly these "standard shot" conditions, a semi-empirical method, discussed in Ref. 2, is used to determine the necessary flow quantities required for data reduction. Some of the data scatter may result from this semi-empirical method which takes into account the slow decay of reservoir conditions with time. Because of this possibility for error, practically all of the results were based on data obtained as close to the peak pressure condition as possible, yet late enough to avoid the transient starting phenomenon. The data point symbol in this report indicates the first usable time point of each run unless specified otherwise.

Since the change in velocity with expansion area ratio is small, most of the results were correlated with free-stream Mach number instead of velocity, the more logical parameter. Figure 14 shows the free-stream Reynolds number per foot achieved as a function of free-stream Mach number where the velocity indicated is practically constant for each data group. The range of Mach number for each of the temperature conditions is limited at present by the quasi-steady flow condition and the minimum machinable tungsten throat diameter.

To give a better understanding of the operating characteristics of Hotshot I in relation to typical hypersonic vehicles under consideration at the present time (Ref. 5), Fig. 15 shows the actual coverage of the present test in terms of density altitude and velocity. This plot gives the conditions under which the velocity (stagnation enthalpy) and free-stream static density are simulated by the experimental data. However, because of the non-simulation of free-static temperature the 4000 and 8000°K conditions result in Mach numbers which are high and low, respectively, for flight simulation. The 6000°K data simulates very closely the free-stream Mach number. Atmospheric properties were taken from Ref. 6.

#### PRECISION

All the basic measured quantities such as pressure, heat transfer, and drag force must be examined for accuracy as affected by:

1. Variation with time
2. Variation between similar runs
3. Variation between transducers
4. Magnitude

The largest variation noted in the measured non-dimensional quantities ( $p_e/P_s$ ,  $\dot{q}/\dot{q}_s$ ) was that associated with run time. This variation, in the case of the pressure transducers, can be traced only to the decay of reservoir conditions. This decay caused a spread in data of less than  $\pm 5$  percent for pressures on the model upstream of the sonic point and generally less than  $\pm 15$  percent on the cylindrical afterbody. A portion of the afterbody data variation may be attributed to difficulties encountered during calibration of the transducer for operation at the extremely low pressures prevalent in this region. The simultaneous measurement of three pressures at  $\theta = 50^\circ$  on three different meridional planes affords a basis for comparing the pressure transducers when operating under approximately the same environment. The variation between transducers was less than  $\pm 6$  percent for all except one run, which showed a single variation of  $\pm 13$  percent. On the afterbody this spread, again because of calibration difficulties, was as much as  $\pm 15$  percent but generally less than  $\pm 9$  percent. Data obtained for each run were, in almost all cases, quite self-consistent; this applies to heat transfer as well. However, the variation between pressure runs with very similar initial conditions resulted in a spread of not more than  $\pm 4$  percent for the forebody and usually less than  $\pm 10$  percent on the afterbody.

The heat gage has associated with it an inherent difficulty which introduces a possibility for error not prevalent in the pressure or drag transducers. Although the design of the gage incorporates the calorimeter principle for operation under dynamic conditions, it is calibrated as a "thin skin" gage. The effect of this deviation on the overall error is not known exactly but it is presumed to contribute significantly. Static calibration can be maintained to within  $\pm 3$  percent. Inaccuracies associated with length of run time are somewhat more complex because of the principle of gage operation and the range of heat transfer rates measured by the gages at different model positions. Although accuracy in the stagnation point region may be affected by possible heat losses through the back of the gage, accuracy on the afterbody may not be so strongly influenced by time but by calibration difficulties encountered when trying to measure rather small quantities. It is not surprising then that the overall error associated with run time is larger than those encountered with pressure measurement. Variations with time, of heat transfer rate ratios ( $\dot{q}/\dot{q}_s$ ) in the stagnation region, were in almost all cases less than  $\pm 12$  percent; whereas, afterbody ratios varied up to  $\pm 25$  percent. Since the variation with time was found to be large, only data near the beginning of the run were felt to be reliable, and these data form the bulk of the heat rate information presented. The spread between similar runs was not easily defined because of the limited amount of data; however, it was probably not greater than  $\pm 10$  percent regardless of location on the hemisphere-cylinder model. Between transducers the spread was less than  $\pm 17$  percent.

Drag coefficients as presented in this report are considered to be within approximately  $\pm 5$  percent except for one run. This estimate includes a partial contribution resulting from the use of free-stream dynamic pressure to convert to drag coefficient.

Shock detachment distance could be measured to within  $\pm 5$  percent.

The determination of aerodynamic and thermodynamic properties for the Hotshot type facility may also contribute to data inaccuracy. These sources of error are discussed in Ref. 2.

The overall accuracy of the data recording system, not including the transducers, is estimated to be better than  $\pm 1.5$  percent.

## RESULTS AND DISCUSSION

Because of the very large cooling rates and low densities in the Hotshot I facility and on the test body, it is appropriate to mention the possible existence of thermal non-equilibrium and rarefied gas effects. Also, because of the relatively short run times and high stagnation temperatures, the ratio of local wall to free-stream enthalpy is approximately 0.02 for the stagnation point and as high as 0.1 for the afterbody regions. Ratios of this order are generally associated with re-entry bodies.

### PRESSURE

Within recent years, experimental investigations (Refs. 7 to 11) have adequately substantiated the validity of the modified Newtonian and later the Newtonian, Matched Prandtl-Meyer (N, P-M) theories for predicting pressure distributions for a fairly broad class of blunt bodies. These investigations also show the asymptotic behavior of the pressure distribution as the Mach number approaches the high supersonic regime. However, afterbody pressure distributions are not amenable to such a simple theoretical prediction at high Mach numbers, and experimental data for Mach numbers greater than 10 in air are rather scarce.

Figure 16 compares a typical pressure distribution obtained on the hemisphere-cylinder in Hotshot I at  $M_\infty = 15.6$  with data from the shock tube (Ref. 7), supersonic (Ref. 8), and hypersonic (Ref. 9) wind tunnels. Although the data cover a rather diverse range of test facilities, the Newtonian and/or N, P-M theories predict the forebody pressure distribution quite accurately.\* However, it is quite evident that as Mach number

---

\*The N, P-M theory for both the Stine-Wanlass and Kubota data has been omitted for the sake of clarity.

increases, the nature of the afterbody pressure distribution changes. The slow decay of pressure on the afterbody is certainly connected with the change in bow-shock shape with increasing Mach number. Therefore, to obtain the true afterbody pressure distribution of hypersonic flight, one must at least simulate the free-stream Mach number, although an asymptotic behavior is again indicated in the data. The blast wave theory (Ref. 9) is not presented in the figure because of its apparent inability to predict the afterbody pressures for small length to diameter ratios. Measurement of afterbody pressures at low Mach numbers and the use of these parameters to predict heat transfer rates will certainly tend to overestimate the rates and reflect themselves in a performance loss of a re-entry body.

Since Refs. 10 and 11 indicated very small Reynolds number effects on the cylindrical afterbody pressures, the comparison of data for the various facilities on the basis of Mach number seems justified; but it is necessary to account for real gas effects, if any.

A specific examination of the Hotshot I data\* reveals a better correlation with the N, P-M theory for  $\gamma = 1.4$  rather than with the expected  $\gamma = 1.2$  theory. The distribution as presented is a function only of instrumentation error and independent of tunnel calibration; and, since correlation with the  $\gamma = 1.4$  theory was substantiated by many other runs (see Fig. 17), the possibility of real gas effects on the forebody was investigated. Using the relaxation times for the various modes of freedom presented in Ref. 12 and the method of this reference for calculating the ratio of times  $\left(\frac{1}{T} \frac{dT}{dt} \tau\right)$ , Fig. 18 was obtained. Assuming the criterion  $\frac{1}{T} \frac{dT}{dt} \tau \leq 10^{-3}$  for equilibrium to be adequate, strong lag effects and possibly frozen flow can be expected to occur beyond  $\theta \gtrsim 50^\circ$  in the inactive degrees of freedom except for  $O_2$  vibration. However, the contribution of  $O_2$  vibration is small. N recombination and NO fixation are not shown since their ratio of times is  $> 10$ . The Mach number chosen for each nominal stagnation temperature presented in Fig. 18 is that which produces the largest densities on the forebody and thus the lower limit of relaxation time.

If one examines the data in terms of  $\tau/\Delta t$  and compares it with the following criteria\*\*, an even earlier onset of frozen flow is indicated (see Appendix A).

---

\*The spread of data indicated in the figure by the bar symbol shows the variation with time during one run as discussed previously.

\*\*These criteria and the analysis given in Appendix A were obtained from work being conducted by Mr. K. Smithson of the Hypervelocity Branch, Gas Dynamics Facility, ARO, Inc.

$$\begin{aligned}\tau/\Delta t &\approx 1, \text{ Lagging} \\ \tau/\Delta t &\leq 10^{-1}, \text{ Equilibrium} \\ \tau/\Delta t &\geq 10^2, \text{ Frozen}\end{aligned}$$

In this case the actual forebody pressure distribution was used to perform the isentropic expansion on a Mollier diagram (Ref. 13) rather than the Newtonian theory as used for Fig. 18.

Figure 17 is a summary plot of the pressure data for the range of Mach number from 11 to 18. To avoid confusion, only three body locations are shown:  $\theta = 50^\circ$ ,  $\theta = 90^\circ$ , and  $s/D = 1.41$ . Even though the data scatter is large, better correlation with the  $\gamma = 1.4$  type flow is evident at  $\theta = 90^\circ$ .

The local-to-stagnation pressure ratio does not appear to be affected by free-stream Mach number over the investigated range. At Mach number 18 a drop in pressure is evident; however, this is attributed to a possible error in recording the body stagnation point pressure for this run. At  $\theta = 50^\circ$  a mean line through the data falls approximately four percent below the modified Newtonian theory,  $p_e/p_s = \cos^2 \theta$ . Rose (Ref. 7) states the adequacy of Newtonian theory for predicting stagnation point velocity gradient for the shock tube as well as for hypersonic flight. The present data, along with others (Ref. 14 and 15), tend to substantiate Rose's conclusion for the hemispherical body.

The Mach numbers for Fig. 17 were determined assuming thermal equilibrium flow upstream of the shock. As will be discussed later (under Shock Detachment), the upstream flow is partially frozen for the three standard shot conditions of this test; however, the equilibrium assumption underestimates the free-stream Mach number at most by five percent.

The local pressures ratioed to free-stream static pressure are presented in Fig. 19 as a function of Mach number. Since it is necessary to consider the chemical state of the flow upstream and downstream of the bow shock when one attempts to form the theoretical ratio  $p_e/p_\infty$ , one may investigate gross effects by analyzing the limit cases of  $\gamma = 1.2$ ,  $\gamma = 1.4$ , and real gas equilibrium.

Although the  $p_e/p_s$  data at  $\theta = 50^\circ$  fell slightly below the Newtonian prediction, the scatter of the  $p_e/p_\infty$  shown in Fig. 19 does not allow forming any quantitative conclusions. Comparison of the data at  $\theta = 90^\circ$  to the completely frozen ( $\gamma = 1.4$ ) and to the equilibrium real gas across the shock with  $\gamma = 1.2$  on the body indicates better agreement with the frozen-flow assumptions.

## HEAT TRANSFER

With the above real gas effects in mind it is now necessary to examine the heat transfer data for similar information as well as Mach number or other effects.

Figure 20 shows the vibration of local-to-stagnation heat transfer ratio as a function of body location on the hemisphere-cylinder. A comparison is made with theory and recent data obtained in the Cornell Aeronautical Laboratory "Tailored-Interface Shock Tunnel" (Ref. 16). The theoretical distribution obtained from the work of Lees (Ref. 17) is shown for both the equilibrium real gas and frozen-flow conditions,  $\bar{\gamma} = 1.4$ . These distributions were computed using the experimental average pressure distribution of Fig. 21 to obtain the local thermodynamic and transport properties. The real gas isentropic expansion was calculated by the same method as discussed under "Pressure"; whereas, following the method suggested by Lees (using an effective  $\bar{\gamma}$ ), the local velocity was related to the experimental pressures through the energy equation. The stagnation point velocity gradient was determined from Newtonian theory. References 18 and 19 were used to calculate the high temperature properties of air.

Since both the CAL and Hotshot I facilities possess similar operating characteristics, the agreement between the data is not surprising. Both distributions fall significantly below the real gas equilibrium theory and show better agreement with the frozen-flow prediction. Again, evidence of non-equilibrium effects is indicated at least beyond the sonic point. One would expect the non-equilibrium effects to decrease as the flow passes on to the afterbody where quasi-constant local flow characteristics are encountered; however, a larger deviation between theory and experiment is evident. Rarefied flow effects can explain decreases of this nature and even though calculations indicate the probable existence of rarefied flow, the data accuracies involved preclude any conclusions to be made in this respect.

Since the hemisphere-cylinder pressure ratio distribution ( $p_e/P_s$ ) was shown to be essentially independent of Mach number for the range of enthalpies covered by the experiment, this same trend is expected to occur in the heat transfer distributions. The variation of local heat transfer ratio as a function of Mach number is given in Fig. 22. Although the data scatter is larger when compared to the pressure results, it is reasonable to conclude a non-dependence of heat transfer on Mach number for the range investigated. For comparison, Lees' theory for the real and  $\bar{\gamma} = 1.4$  gas flow is used. No definite conclusions can be drawn regarding the correlation of data with theory at  $\theta = 50^\circ$  because of scatter. However, at the juncture ( $\theta = 90^\circ$ ) the mean line of the data scatter is at least 40 percent lower than the thermal equilibrium theory, and since this deviation is somewhat greater than the average data scatter, one can assume the better correlation with

frozen-flow conditions to be significant. On the afterbody the average data line is approximately 50 percent lower than equilibrium theory.

Figure 23 is a plot of the absolute value of stagnation point heat transfer rate versus free-stream Mach number. Although these rates are of little use for scaling to actual hypersonic flight, a comparison with theory can be made. The scatter of measured rates is greater than the spread between the Lees  $\bar{\gamma} = 1.2$  and Fay-Riddell  $L = 1.4$  (Ref. 20) thermal equilibrium theories. The only observation which can be made is that the general trend of the data is in agreement with theory.

Probstein (Ref. 21) shows that the stagnation point heat transfer on a blunt body is strongly influenced by the proper choice of the  $\rho\mu$  product across the boundary layer. His analysis indicates the necessity of using a realistic variation of  $\rho\mu$  through the boundary layer rather than the  $\rho\mu$  product at the wall. A significant reduction in heat transfer is apparent when the realistic variation of  $\rho\mu$  is used. Comparison of the present data with theory in terms of  $Nu_w/\sqrt{Re_w}$  and the boundary layer fluid properties ( $\rho\mu$ ) is presented in Fig. 24. Again the data scatter is too large to permit any quantitative comments beyond general trend agreement. The Fay-Riddell equilibrium theory for  $L = 1.4$  and  $1.0$  is that of Ref. 20 and the Lees-Probstein curve is that of Lees (Ref. 17) as defined by Probstein (Ref. 21). In order to verify the theoretical predictions of  $Nu_w/\sqrt{Re_w}$  with the  $\rho\mu$  product it will be necessary to refine considerably the measurement accuracy of the heat transfer gage.

## DRAG

Drag coefficients measured with the one-component axial force balance are compared with theory and other experimental data in Fig. 25. The force measurements, which could include possible rarefied flow and base pressure effects, can be compared to the drag obtained from integration of the experimental pressure distributions. The average of the force measurements lies approximately ten percent above the integrated pressure drag. Since the base pressure is estimated to contribute less than one percent to the overall drag coefficient, this increase can be attributed mainly to skin friction. Estimates of skin friction based on the Cohen-Reshotko (Ref. 22) theory (assuming continuum flow) account for a maximum contribution of  $\approx 4$  to 9 percent. It was also estimated that the effect of the slightly flared drag-model afterbody (mentioned under "Models") contributed less than a one percent increase to the overall drag coefficient.

Figure 25 also reveals that the Newtonian theory,  $C_D = C_{p_{max}}/2$ , estimates the forebody pressure drag to within approximately three percent.

The value of  $C_{p_{max}}$  for this estimate was the average of the experimental values obtained during the pressure tests. Even though it has been shown that Newtonian theory underestimates the pressure aft of the sonic point, it still predicts the forebody drag adequately. This is due to the decreasing contribution of the pressure drag component as the juncture is approached. Liu (Ref. 23), on the other hand, assumed the forebody drag on a sphere to be dictated by the local pressure behind a closely wrapped bow shock; he also assumed no skin friction components. With these assumptions he shows good agreement with Hodges (Ref. 24) in the Mach number range from 5 to 10. The latter data were obtained in air on a ballistic range. Because of the high Reynolds numbers the effects of skin friction might be considered small. Liu's theoretical model is not unlike the conditions of the present study except for skin friction. The deviation between Liu's theory and the drag balance coefficients is approximately the same as that between the balance data and the integrated pressure drag. This comparison fortifies the assumption of significant skin friction effects.

As mentioned earlier in the report, relaxation effects upstream of the bow shock can cause errors in the calculation of free-stream conditions. Since the drag coefficient is a function of the free-stream dynamic pressure it is necessary to estimate what effect, if any, the assumption of thermal equilibrium might have on calculating  $C_D$ . Analysis of the flow in the nozzle, allowing for relaxation effects, indicates that the test section static density can be underestimated by as much as nine percent and the velocity overestimated by approximately four percent if thermal equilibrium is assumed. It is evident, therefore, that the product  $\rho_\infty u_\infty^2$  (proportional to dynamic pressure) is practically unaffected. Thus the drag coefficient as determined should be subject only to drag balance and tunnel calibration errors.

## SHOCK DETACHMENT

The investigation of shock detachment distance for blunt bodies has received much attention recently because of its use in the study of real gas effects (Refs. 25 and 26). Shock detachment distance was considered to be of secondary importance until the occurrence of unexpected trends was noted. An attempt to clarify these trends led to the investigation of possible thermal non-equilibrium effects which can cause, as has been shown both theoretically and experimentally (Refs. 25 and 26), large deviations in the shock standoff distance. The present knowledge of relaxation phenomena does not allow accurate predictions to be made; therefore, the following discussion is included to lend possible explanation to the noted trends and is not intended to verify any theories.

Figure 26 is a plot of shock detachment distance as a function of Mach number. The latter parameter was used rather than the normal shock density ratio (as suggested by theory) because it is believed that a greater degree of accuracy can be achieved in view of the possible non-equilibrium effects. The relaxation analysis of the nozzle flow is felt to be more reliable than that for the downstream side of the shock (to be discussed later in this section). Listed in the following table are the frozen energies in the nozzle for the three standard expansions in percent of stagnation enthalpy, \*

	4000°K	6000°K	8000°K
N <sub>2</sub> Vibration	2.9%	2.7%	2.3%
O <sub>2</sub> Vibration	0.4	0.3	--
NO Inactive	4.6	2.4	1.0
O Inactive	--	1.3	5.7
N Inactive	--	--	0.5
Total	7.9%	6.7%	9.5%

The analysis indicated the flow to be frozen at a short distance ( $\leq 1$  in.) downstream of the throat.

Serbin's theory (Ref. 27), although for  $\gamma \rightarrow 1$  and large  $\rho_2/\rho_1$ , shows fair agreement with the various data obtained in diatomic gases (Refs. 10, 14, 27, and 28); whereas, a larger deviation is noted when compared to monatomic gas data (Ref. 26). However, the theory is used to indicate the variation of  $\delta/R_N$  to be expected for various participating degrees of freedom.

The Hotshot I data for 8000°K indicate a rather precipitous transition from equilibrium to the frozen-flow state, while this transition at 6000°K is more gradual. For the lower portion of the 4000°K Mach number range, the data indicate a vibrational equilibrium state and a gradual transition to a frozen state as the Mach number increases. One might expect that if the reservoir temperature is increased to say 10,000°K, holding the density constant, the variation of  $\delta/R_N$  would fall along the  $\gamma = 1.2$  line; whereas, decreasing the temperature at constant density, one could certainly expect correlation with the  $\gamma = 1.4$  prediction.

---

\*Taken from the work of H. K. Smithson (previously cited).

It is now necessary to examine relaxation effects downstream of the shock to determine whether any correlation exists between the data trends and relaxation estimates. Since the calculation of relaxation effects in the stagnation region is complex, one can compare on a simplified basis the transit to relaxation time in this region when an average velocity from the shock to the body is assumed. Table 1, using the relaxation data of Ref. 12, is based on calculations made for each individual run and indicates qualitatively the presence of non-equilibrium effects.

On the basis of the qualitative data in Table 1, it may be explained that for the 4000°K case the only inactive participating degree of freedom is vibration; thus  $\gamma$  could have the value 1.286. As the nominal temperature is raised above 4000°K towards 8000°K the  $(\partial E / \partial T)_v$  increases because of dissociation. The equilibrium values of  $\gamma$  in this range of temperature and  $10^{-2}$ -atm density fall between 1.17 and 1.25. However, a decrease in density by approximately one order of magnitude with increasing Mach number is associated with each individual standard expansion. Since this decrease in density can increase relaxation times by one or more orders of magnitude, one might expect the trend to be towards frozen flow with increasing Mach number for each standard expansion.

Several factors which contribute to the inability to predict relaxation effects are: (1) the uncertainty connected with basic relaxation time estimates, (2) arc chamber contaminants where small amounts can cause variations in relaxation time estimates, and (3) extrapolation of relaxation time information.

Because of the low densities, the order of  $10^{-3}$  atm, and high test section velocities, the analysis of Adams and Probst (Ref. 29) was used to examine rarefied gas effects in the model stagnation region. For the stagnation region of the models tested, the results indicate that:

1. Continuum flow theory was applicable
2. Slip flow was not present
3. The boundary layer thickness was much less than the shock detachment distance
4. The shock thickness was less than the boundary layer thickness

An independent calculation using the theory of Ref. 22 indicated that the boundary layer displacement thickness was less than 1/20 of the shock detachment distance ( $\delta$ ) for the adiabatic wall case. Therefore one concludes that  $\delta^* < \delta$  for the "cold wall" condition.

## CONCLUSIONS

An experimental investigation was conducted in the AEDC Hotshot I facility to determine the pressure and heat transfer distributions, drag, and shock detachment distance of a hemisphere-cylinder in the Mach number range from 11 to 18. The data are compared with theory and other experimental results and an attempt is made to explain deviations between theory and experiment. The results of this investigation indicate that:

1. The Newtonian, Matched Prandtl-Meyer theory is adequate for predicting the hemispherical pressure distribution at hypersonic velocities. Better correlation with theory is obtained when a  $\gamma = 1.4$  flow is assumed indicating the possibility of relaxation effects on the forebody.
2. The pressure and heat transfer distributions on the body are found to be essentially independent of free-stream Mach number and stagnation enthalpy for the range covered by the experiment.
3. The heat transfer distributions fall below Lees' theory and the deviation increases with distance from the body stagnation point. Beyond approximately the sonic point the data are found to correlate with the  $\gamma = 1.4$  theory rather than with the real gas analysis indicating again the possibility of thermal non-equilibrium effects.
4. Because of scatter of the stagnation point heat transfer data, it is not possible to form any quantitative conclusions. Only agreement in general trend is noted with the Fay-Riddell and Lees theories.
5. The drag balance measurements result in drag coefficients which are approximately ten percent larger than the integrated pressure distributions or Newtonian theory; this discrepancy is almost completely attributed to skin friction. The drag coefficient is found to be practically independent of free-stream Mach number and stagnation enthalpy with a value of  $\approx 1.05$  based on frontal area.
6. The shock detachment data are subject to speculation. Trends in the data indicate the possibility of thermal non-equilibrium effects; however, more definite data are required before sound conclusions can be made. Serbin's theory for shock detachment is used to evaluate the data trends.

## REFERENCES

1. MacDermott, W. N. "Preliminary Test Results with an Arc Heated Hypersonic Wind Tunnel at Mach Numbers of 10 to 20." Proceedings of the Fifth Midwestern Conference on Fluid Mechanics, University of Michigan Press, 1957.
2. Perry, R. W. and MacDermott, W. N. "Development of the Spark-Heated, Hypervelocity, Blowdown Tunnel - Hotshot." AEDC-TR-58-6, June 1958.
3. Mulkey, M. R., Earheart, W. T., Jr., and McAdams, E. E., Jr. "Pressure Measurements in an Arc-Discharge Wind Tunnel." AEDC-TN-58-16, April 1958.
4. Rose, P. H. "Development of the Calorimeter Heat Transfer Gage for Use in Shock Tubes." AVCO Research Report 17, February 1958.
5. Masson, D. J. and Gazley, C., Jr. "Surface-Protection and Cooling Systems for High Speed Flight." Aeronautical Engineering Review, Vol. 15, November 1956, pp. 46-55.
6. Ramo-Woolridge Corporation. "An Approximate ICAO 1956 Atmosphere." GM-TR-173, January 1957.
7. Rose, P. H. "Physical Gas Dynamics Research at the AVCO Research Laboratory." AVCO Research Note No. 37, May 1957.
8. Stine, H. A. and Wanlass, K. "Theoretical and Experimental Investigation of Aerodynamic-Heating and Isothermal Heat Transfer Parameters on a Hemispherical Nose with Laminar Boundary Layer at Supersonic Mach Numbers." NACA TN 3344, December 1954.
9. Kubota, T. "Investigation of Flow around Simple Bodies in Hypersonic Flow." Guggenheim Aeronautical Laboratory, California Institute of Technology, CIT Memo No. 40, June 1957.
10. Oliver, R. E. "An Experimental Investigation of Flow over Simple Blunt Bodies at a Nominal Mach Number of 5.8." CIT Memo No. 26, June 1955.
11. Crawford, D. H. and McCauley, W. D. "Investigation of the Laminar Aerodynamic Heat-Transfer Characteristics of a Hemisphere-Cylinder in the Langley 11-inch Hypersonic Tunnel at a Mach Number of 6.8." NACA TN 3706, July 1956. (Superseded by NACA Report 1323, 1957.)
12. Logan, J. G., Jr. "Relaxation Phenomena in Hypersonic Aerodynamics." Institute of the Aeronautical Sciences Preprint No. 728, January 1957.

13. AVCO Research Laboratory. "Mollier Diagram for Equilibrium Air." January 1957.
14. Boison, J. C. and Curtiss, H. C. "Preliminary Results of Spherical-Segment Blunt Body Surveys in the 20-inch Supersonic Wind Tunnel at JPL." AVCO RAD-2-TM-57-77, October 1957.
15. Korobkin, I. and Gruenewald, K. H. "Investigation of Local Laminar Heat Transfer on a Hemisphere for Supersonic Mach Numbers at Low Rates of Heat Flux." Journal of the Aeronautical Sciences, Vol. 24, March 1957, pp. 188-194.
16. Wittliff, C. E., Wilson, M. R., and Hertzberg, A. "The 'Tailored-Interface' Hypersonic Shock Tunnel." CAL, Paper Presented at ASME-ARS Aviation Conference, Dallas, Texas, March 1958.
17. Lees, L. "Laminar Heat Transfer over Blunt-Nosed Bodies at Hypersonic Flight Speeds." Jet Propulsion, Vol. 26, April 1956, pp. 259-269, 274.
18. Hilsenrath, J. and Beckett, C. W. "Tables of Thermodynamic Properties of Argon-Free Air to 15,000°K." AEDC-TN-56-12, September 1956.
19. Logan, J. G., Jr. "Thermodynamic Charts for High Temperature Air Calculation." CAL Report No. AD-1052-A-3, July 1956.
20. Fay, J. A. and Riddell, F. R. "Theory of Stagnation Point Heat Transfer in Dissociated Air." Journal of Aeronautical Sciences, Vol. 25, February 1958, pp. 73-85, 121.
21. Probstein, R. F. "Method of Calculating the Equilibrium Laminar Heat Transfer Rate at Hypersonic Flight Speeds." Technical Note, Jet Propulsion, Vol. 26, June 1956, pp. 497-499.
22. Cohen, C. B. and Reshotko, E. "Similar Solutions for the Compressible Laminar Boundary Layer with Heat Transfer and Pressure Gradient." NACA Technical Report 1293, 1956.
23. Liu, V. C. "On the Drag of a Sphere at Extremely High Speeds." Journal of Applied Physics, Vol. 29, February 1958, pp. 194-195.
24. Hodges, A. J. "The Drag Coefficient of Very High Velocity Spheres." Journal of the Aeronautical Sciences, Vol. 24, October 1957, pp. 755-758.
25. Bray, K.N.C. "Departure from Dissociation Equilibrium in a Hypersonic Nozzle." ARC 19,983, March 1958.
26. Schwartz, R. N. and Eckerman, J. "Shock Location in Front of a Sphere as a Measure of Real Gas Effects." Journal of Applied Physics, Vol. 27, February 1956, pp. 169-174.

27. Serbin, H. "Supersonic Flow around Blunt Bodies." Journal of the Aeronautical Sciences, Vol. 25, January 1958, pp. 58-59.
28. Lees, L. "Recent Developments in Hypersonic Flow." Jet Propulsion, Vol. 27, November 1957, pp. 1162-1178.
29. Adams, M. C. and Probst, R. F. "On the Validity of Continuum Theory for Satellite and Hypersonic Flight Problems at High Altitudes." Jet Propulsion, Vol. 28, February 1958, pp. 86-89.
30. Herzfeld, K. F. "Relaxation Phenomena in Gases." Section H, Vol. I, Thermodynamics and Physics of Matter, Princeton University Press, 1955.



## APPENDIX A

For small deviations from equilibrium the relaxation equation is (Ref. 30)

$$\frac{\partial E'}{\partial t} = -\frac{1}{\tau} [E' - E'_{(tr)}] \quad (1)$$

where  $E'$  is the energy of the internal degree of freedom,  $E'_{(tr)}$  is the equilibrium energy of the internal degree of freedom at  $T_{tr}$  (temperature of the translational degree of freedom).

Integrating (1) between the limits of  $E'_{(x_1)}$  and  $E'_{(x_2)}$ ; and  $t_1$  and  $t_2$  we obtain

$$E_{x_2}' = \frac{1}{e^{-\frac{\Delta t}{\tau}}} \left[ E_{x_1}' - E'_{(tr)_{x_2}} \right] + E'_{(tr)_{x_2}} \quad (2)$$

where  $t_2 - t_1 = \Delta t$  and  $x_1, x_2$  are two arbitrary spacial locations.

### EQUILIBRIUM FLOW

For values of  $\frac{\Delta t}{\tau} \geq 10$ ,  $e^{-\frac{\Delta t}{\tau}} < 0(10^{-4})$  thus

$$e^{-\frac{\Delta t}{\tau}} \left[ E_{x_1}' - E'_{(tr)_{x_2}} \right] \rightarrow 0$$

and  $E'_{x_2} \approx E'_{(tr)_{x_2}}$

### FROZEN FLOW

For values of  $\frac{\Delta t}{\tau} \leq 10^{-2}$ ,  $e^{-\frac{\Delta t}{\tau}} > .99$

thus  $E_{x_2}' \rightarrow E_{x_1}'$  and the degree of freedom will be frozen.

### RELAXING FLOW

For  $10 \geq \frac{\Delta t}{\tau} \geq 10^{-2}$ ,  $E_{x_2}'$  will assume a value between equilibrium and frozen flow where the inactive degree of freedom will partially adjust toward equilibrium.

TABLE 1

SUMMARY OF QUALITATIVE ANALYSIS OF RELAXATION PHENOMENA  
IN STAGNATION REGION OF HEMISPHERE-CYLINDER MODELS TESTED IN  
HOTSHOT I

$T_{o_{nom}}, ^\circ K$	$O_2$ vib.	$N_2$ vib.	$N_{diss.}$	$O_{diss.}$	NO
4000	equilibrium or relaxing	relaxing or frozen	frozen*	frozen*	frozen
6000	probably in equilibrium	relaxing	frozen	relaxing	relaxing or frozen
8000	equilibrium or relaxing	equilibrium or relaxing	frozen	relaxing	relaxing or frozen

\*The equilibrium concentration of these degrees of freedom for the conditions of this expansion are practically negligible.

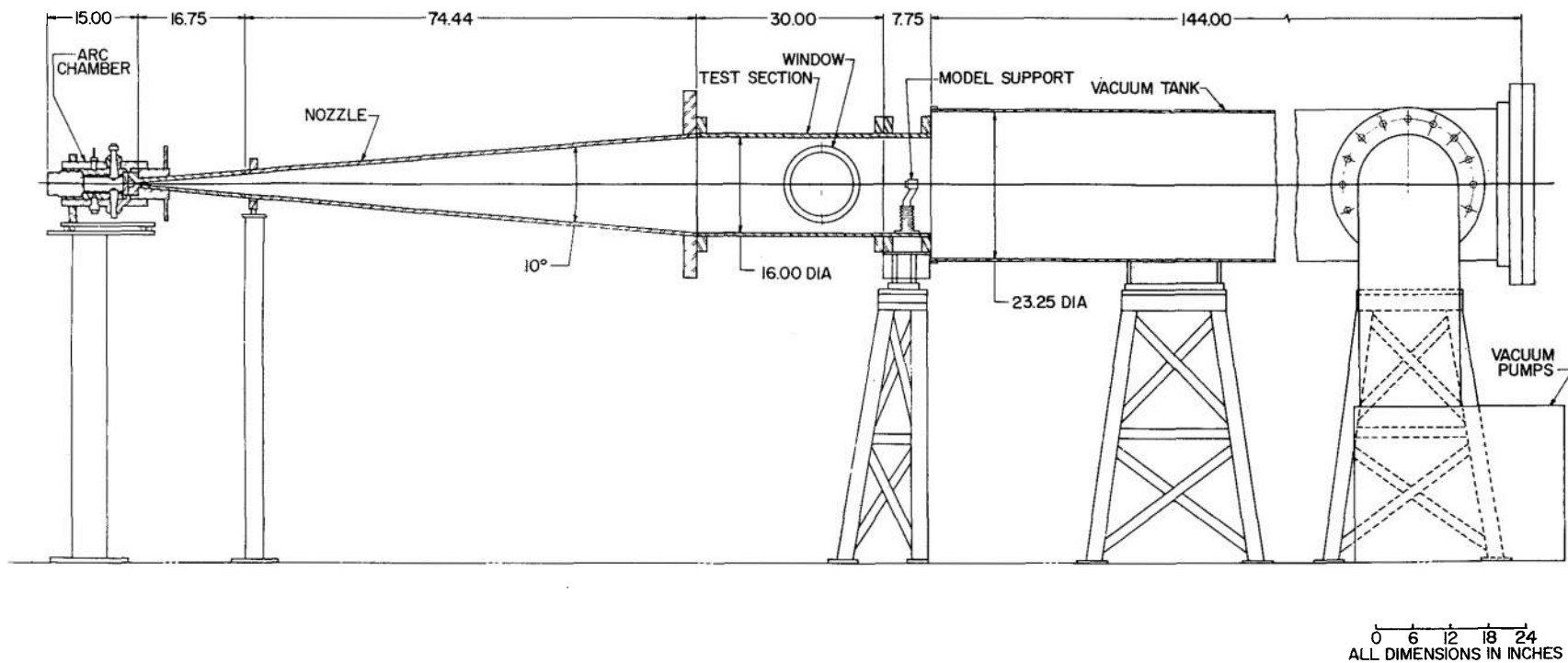


Fig. 1. Hotshot I Schematic

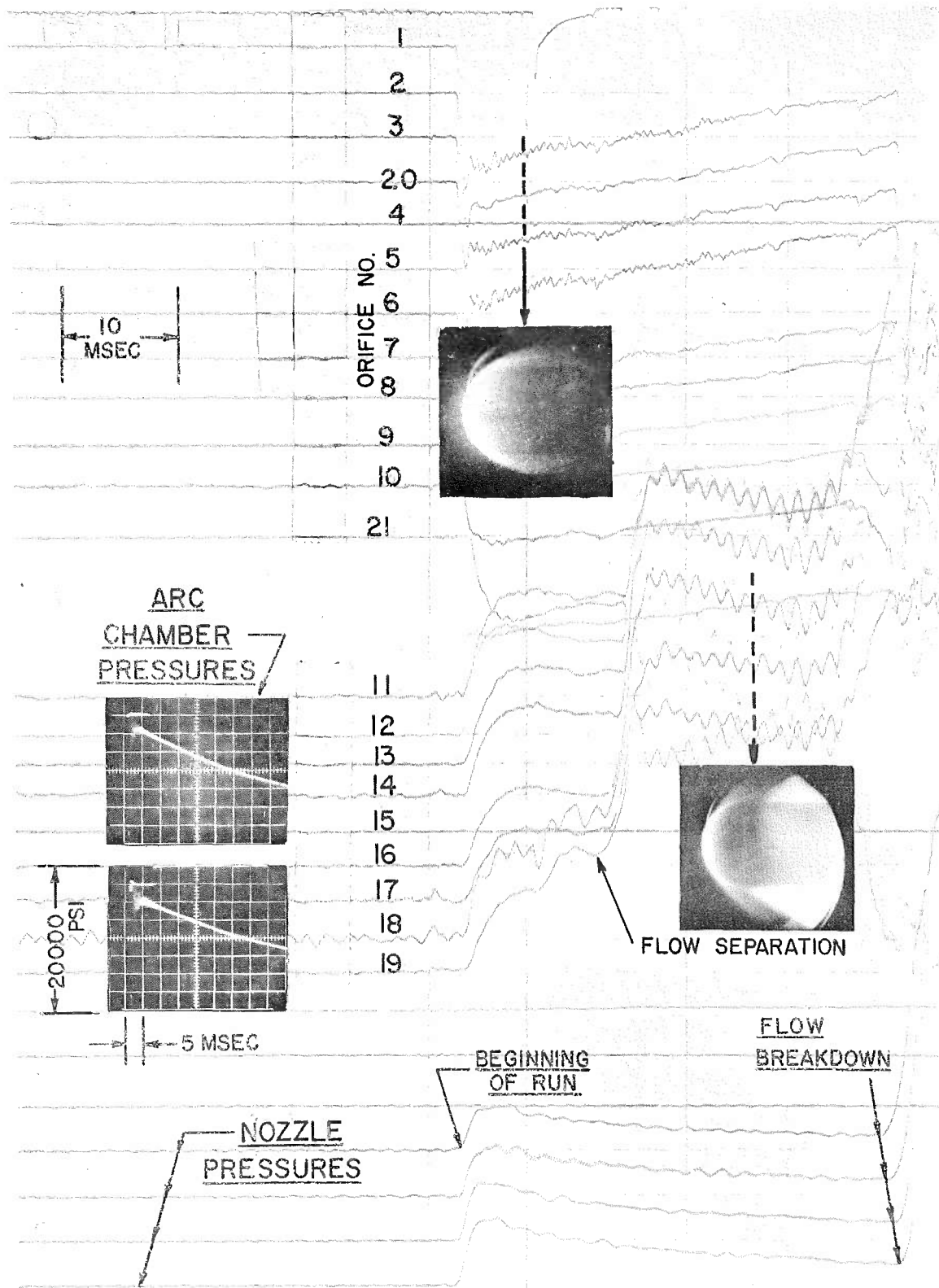


Fig. 2. Typical Raw Data - Pressure

Model Position	1	20	2-3	4-5	6-7-21	8-9	10-11	12-13	14-15	16-17	18-19
$\theta^\circ$	0	10	15	30	50	70	90	--	--	--	--
s/D	0	.0873	.1309	.2618	.4363	.6109	.7854	.9104	1.1604	1.4104	1.6604

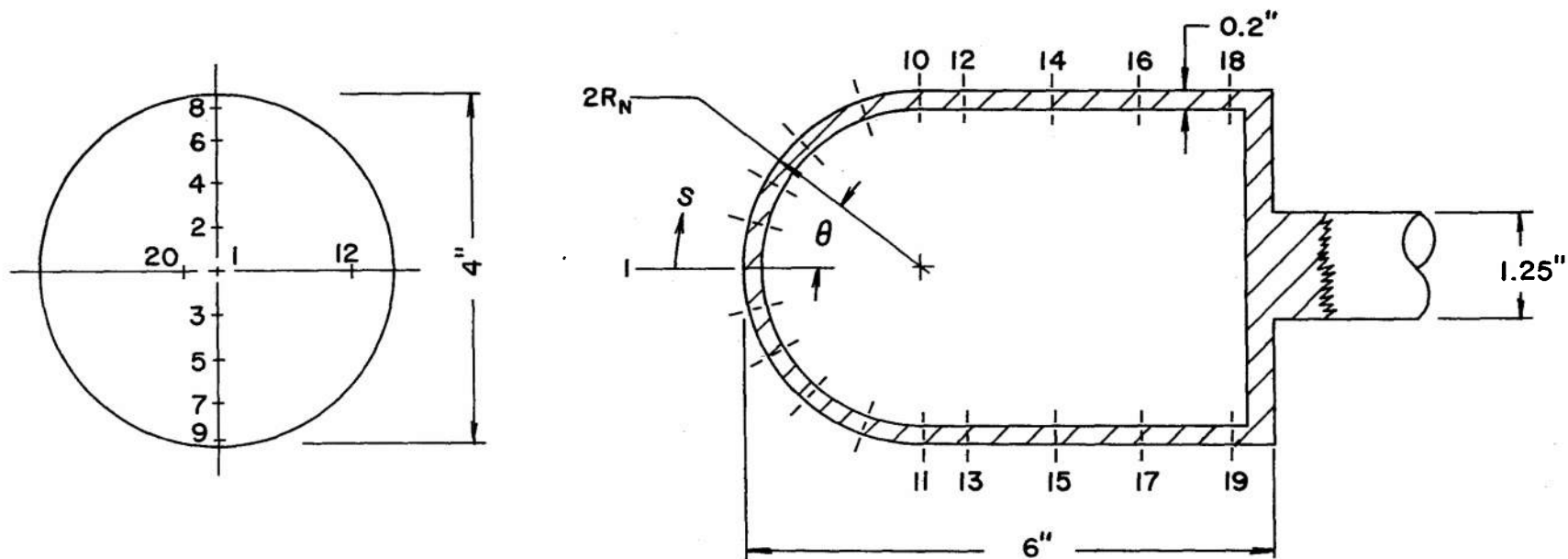
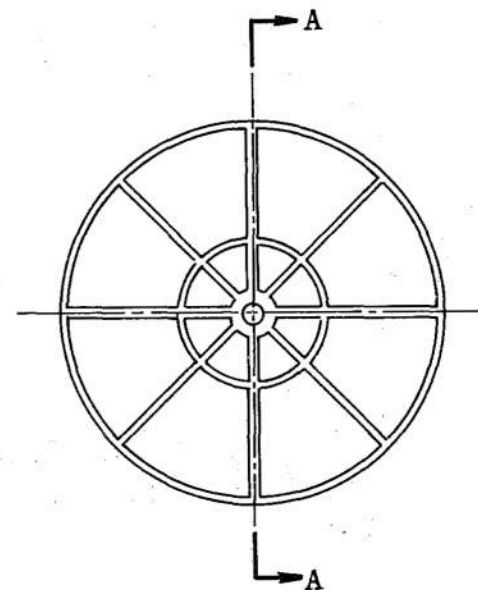
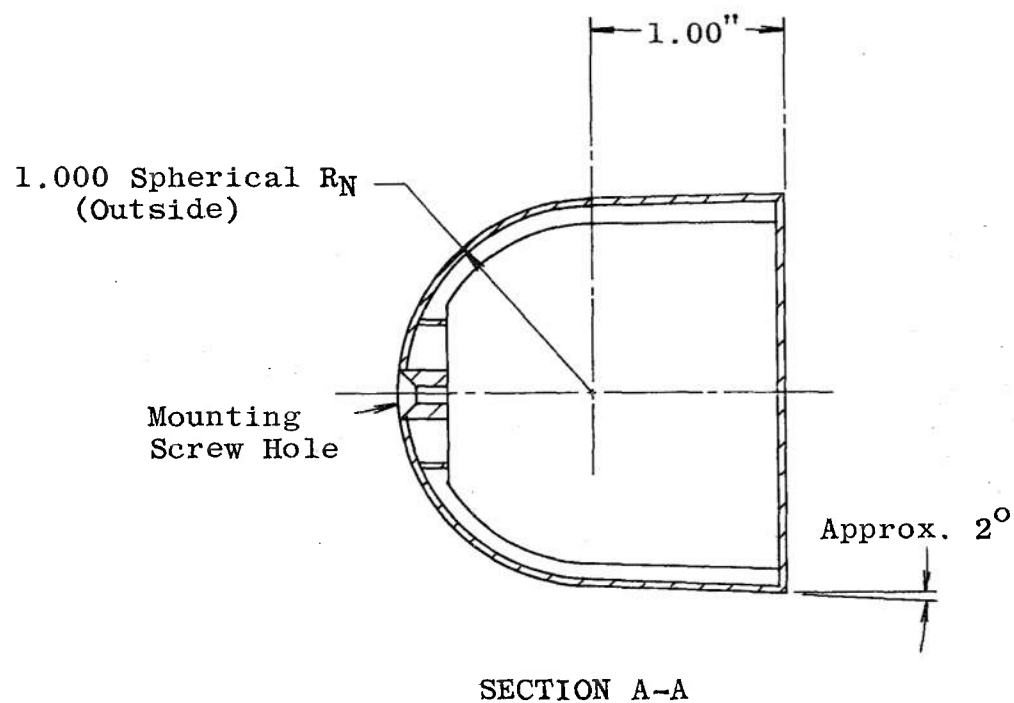


Fig. 3. Hemisphere-Cylinder Model Dimensions



- Notes: 1. All walls and webs 0.031" thick  
2. Material - fiberglass

Fig. 4. Hemisphere-Cylinder Drag Model (Schematic)

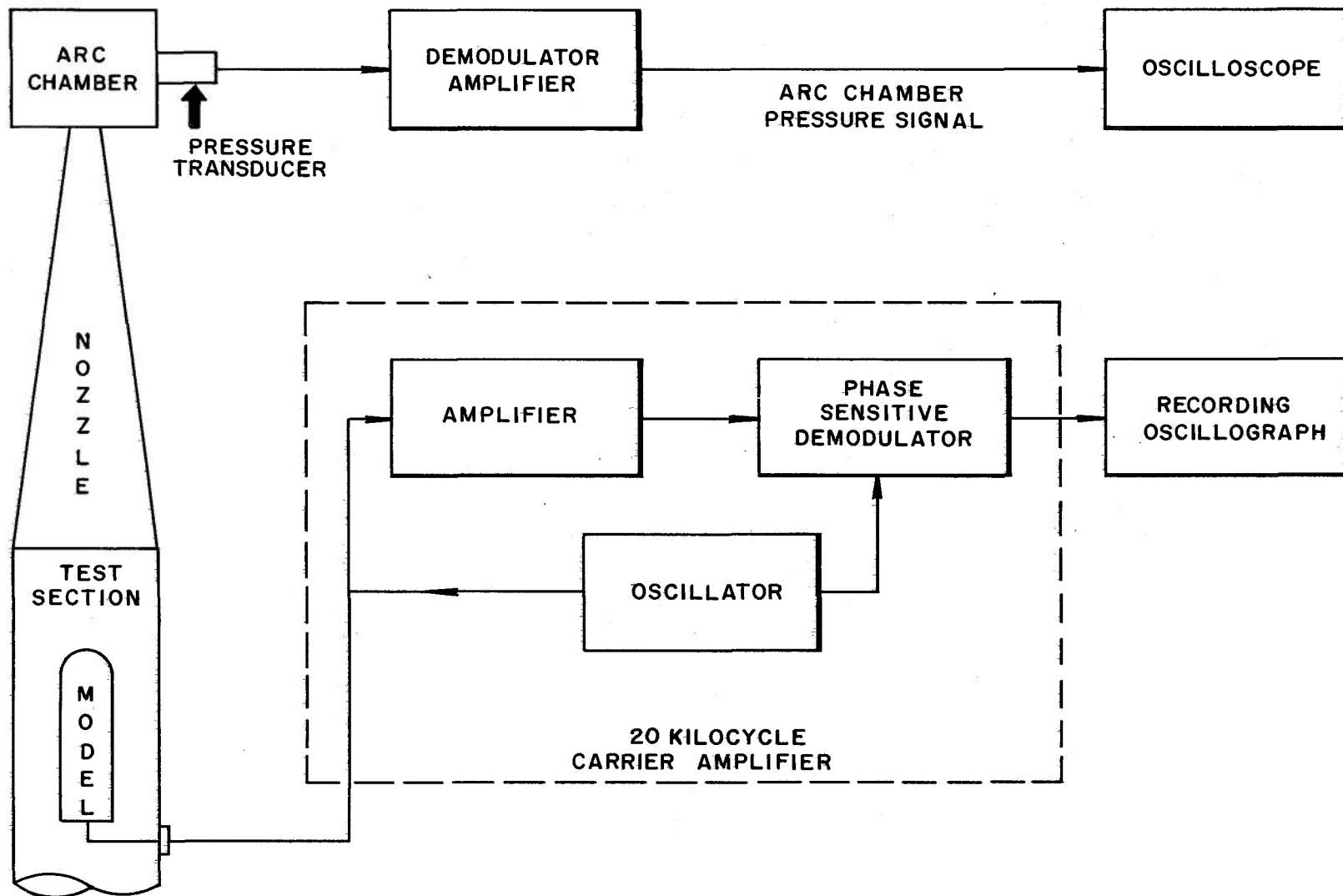


Fig. 5. Schematic of Data Recording System

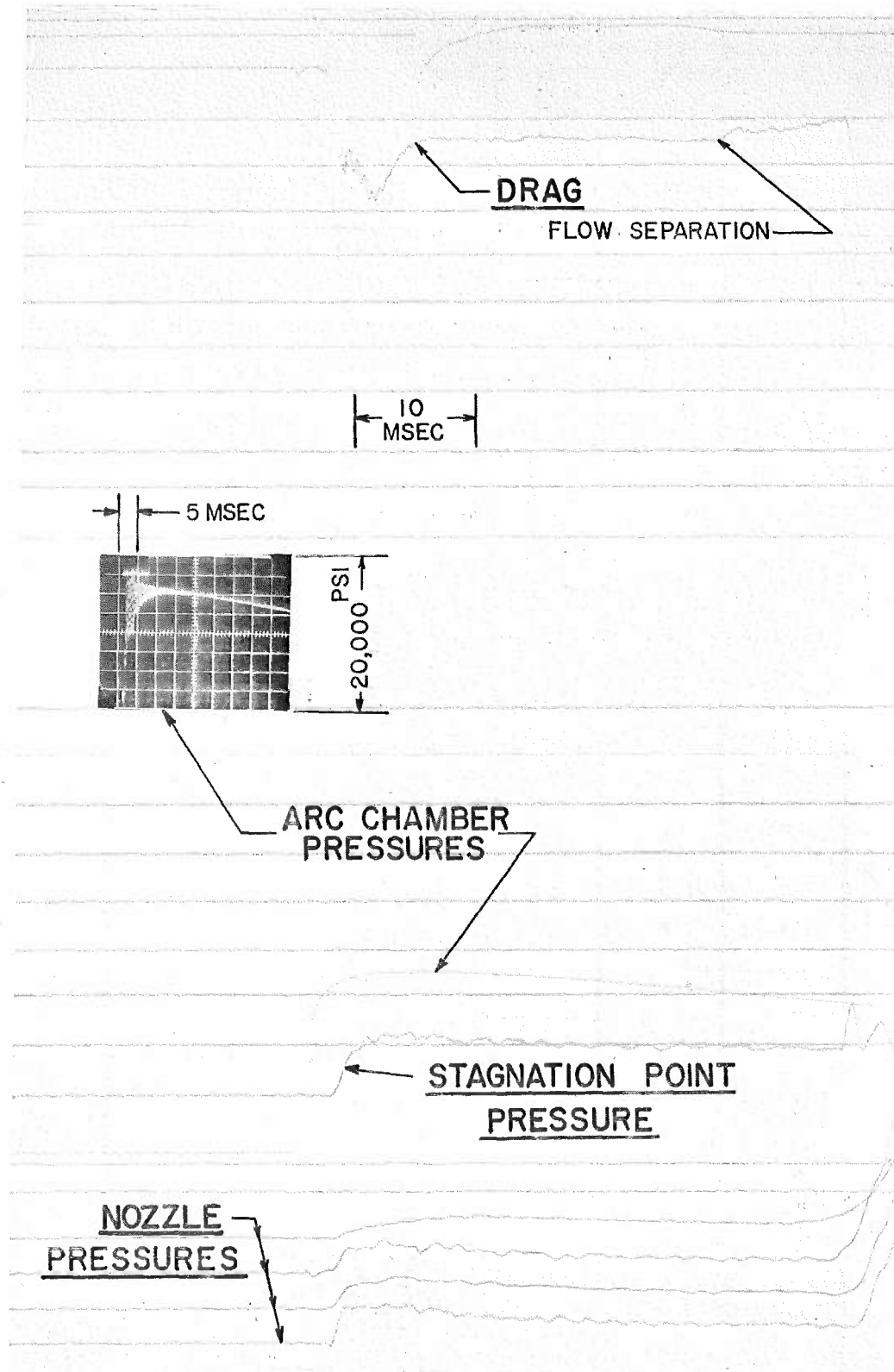


Fig. 6. Typical Raw Data - Drag

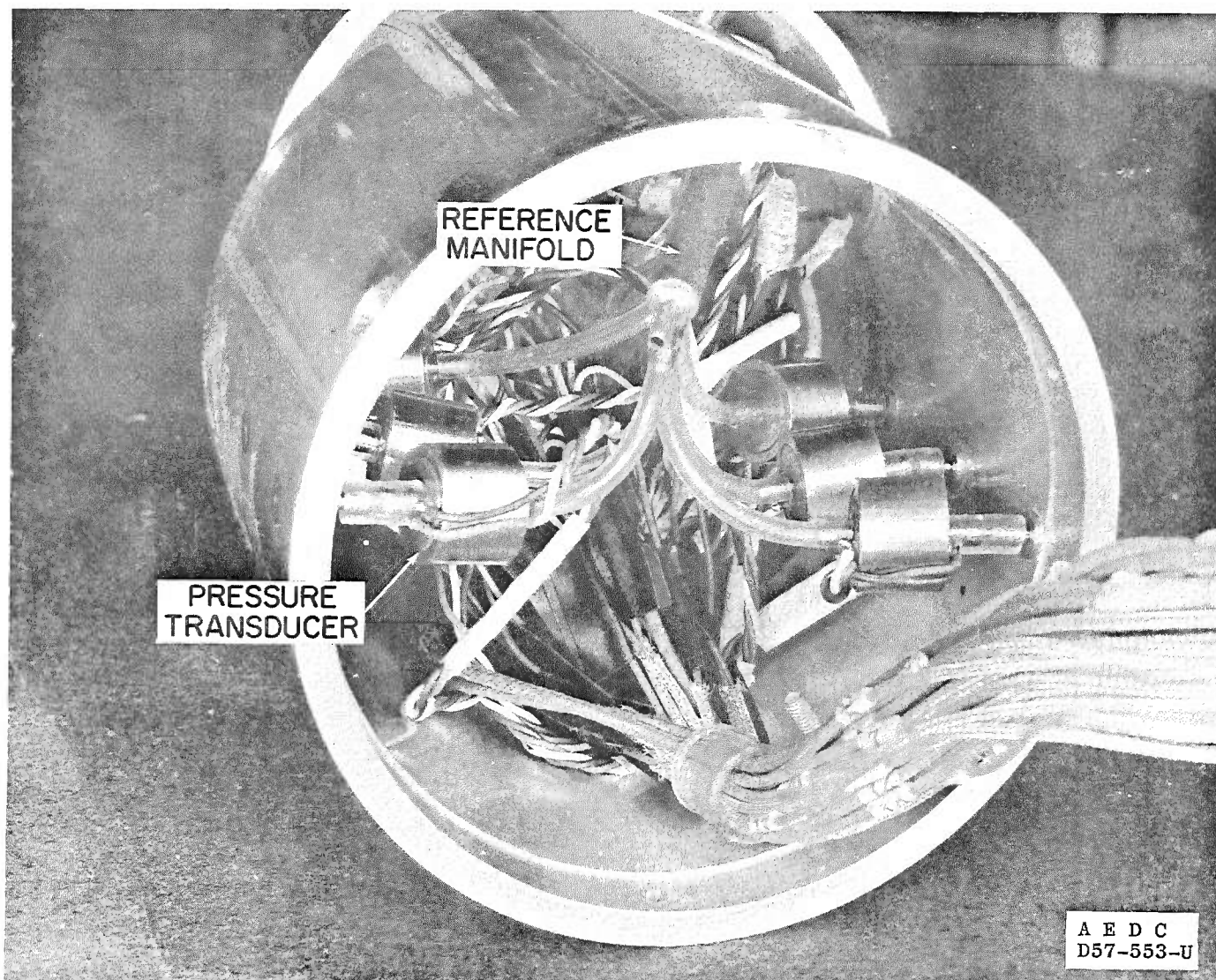


Fig. 7. Hemisphere-Cylinder Pressure Transducer Installation

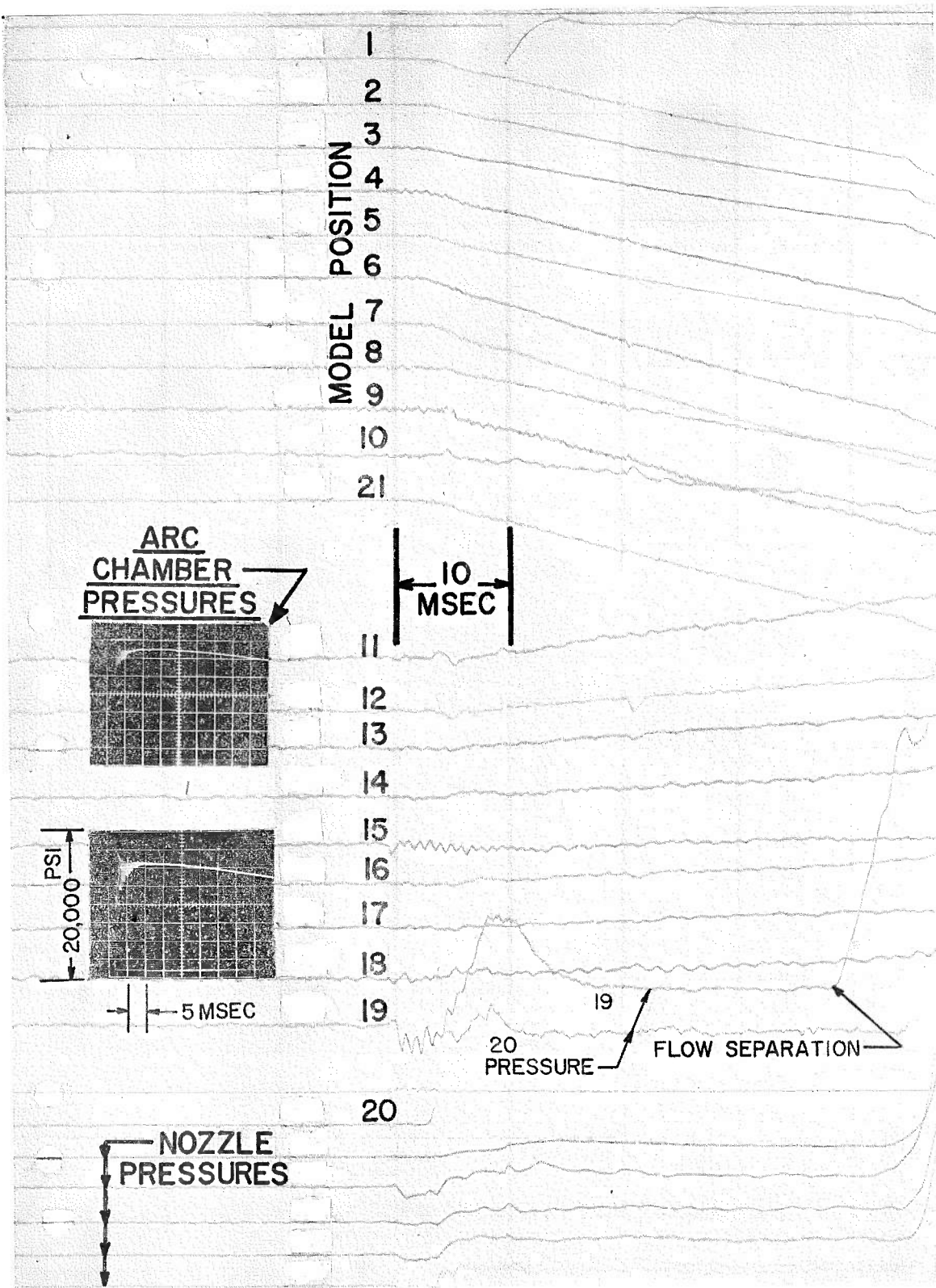


Fig. 8. Typical Raw Data - Heat Transfer

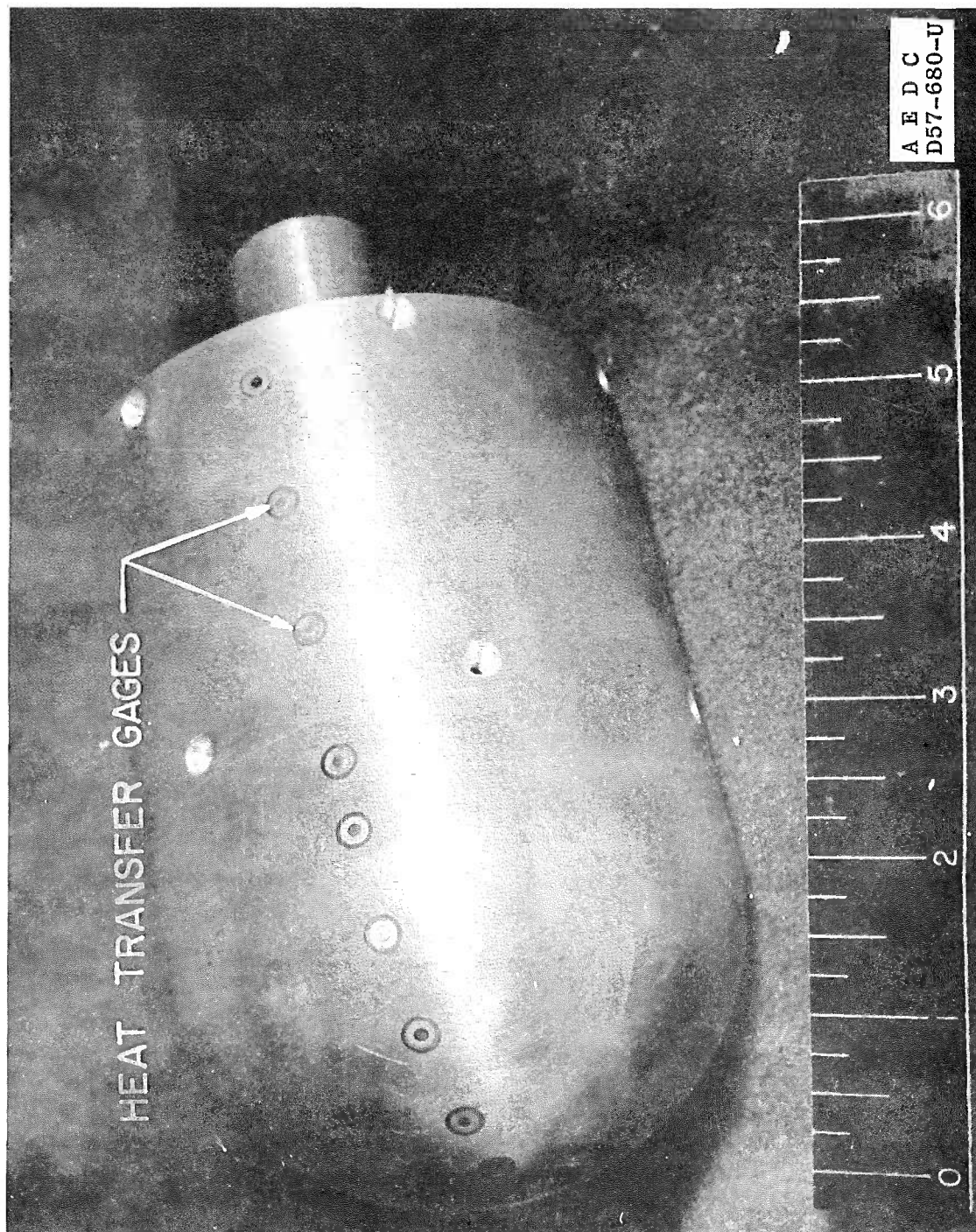


Fig. 9. Hemisphere-Cylinder Heat Transfer Model

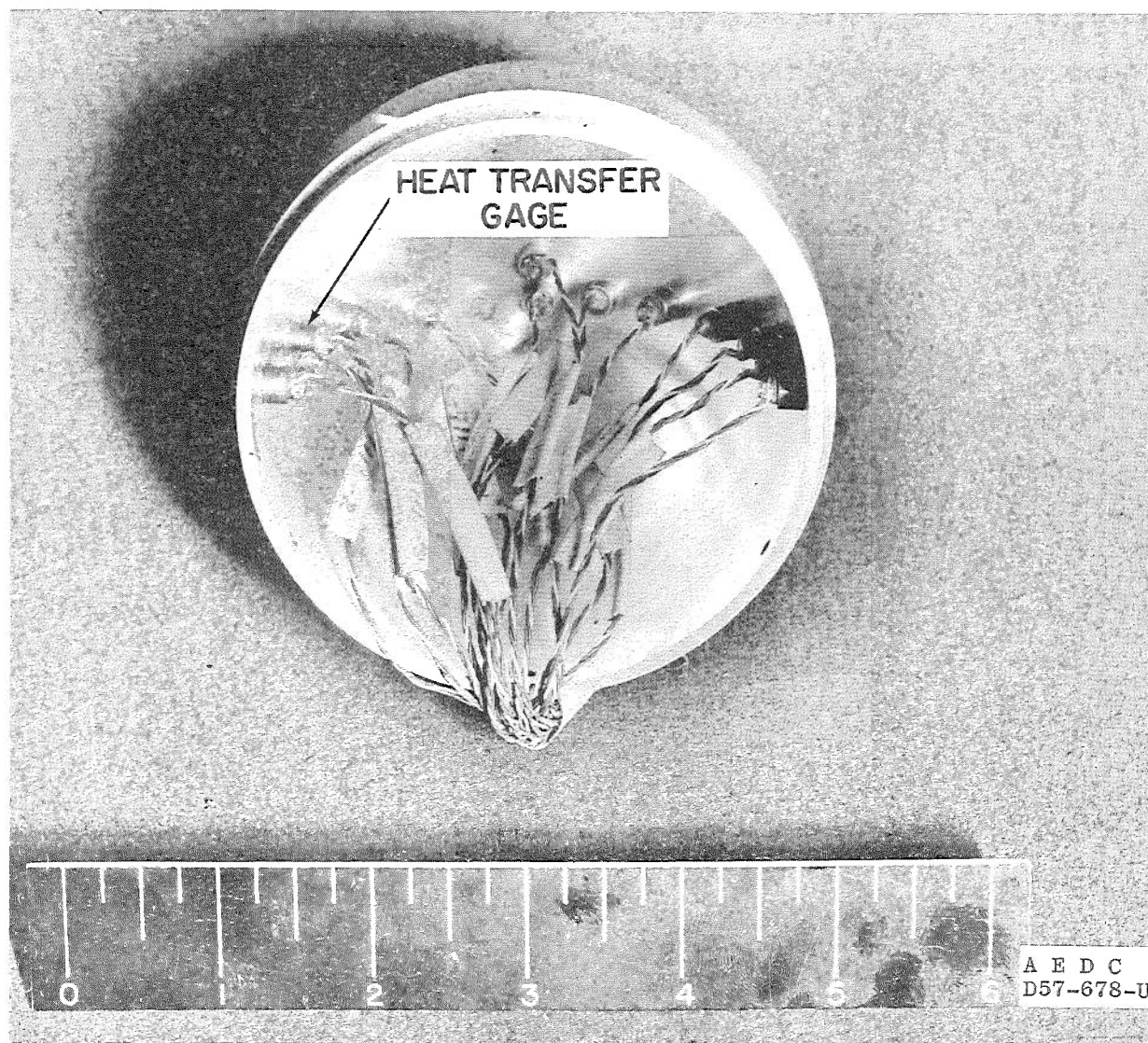


Fig. 10. Hemisphere-Cylinder Heat Transfer Gage Installation

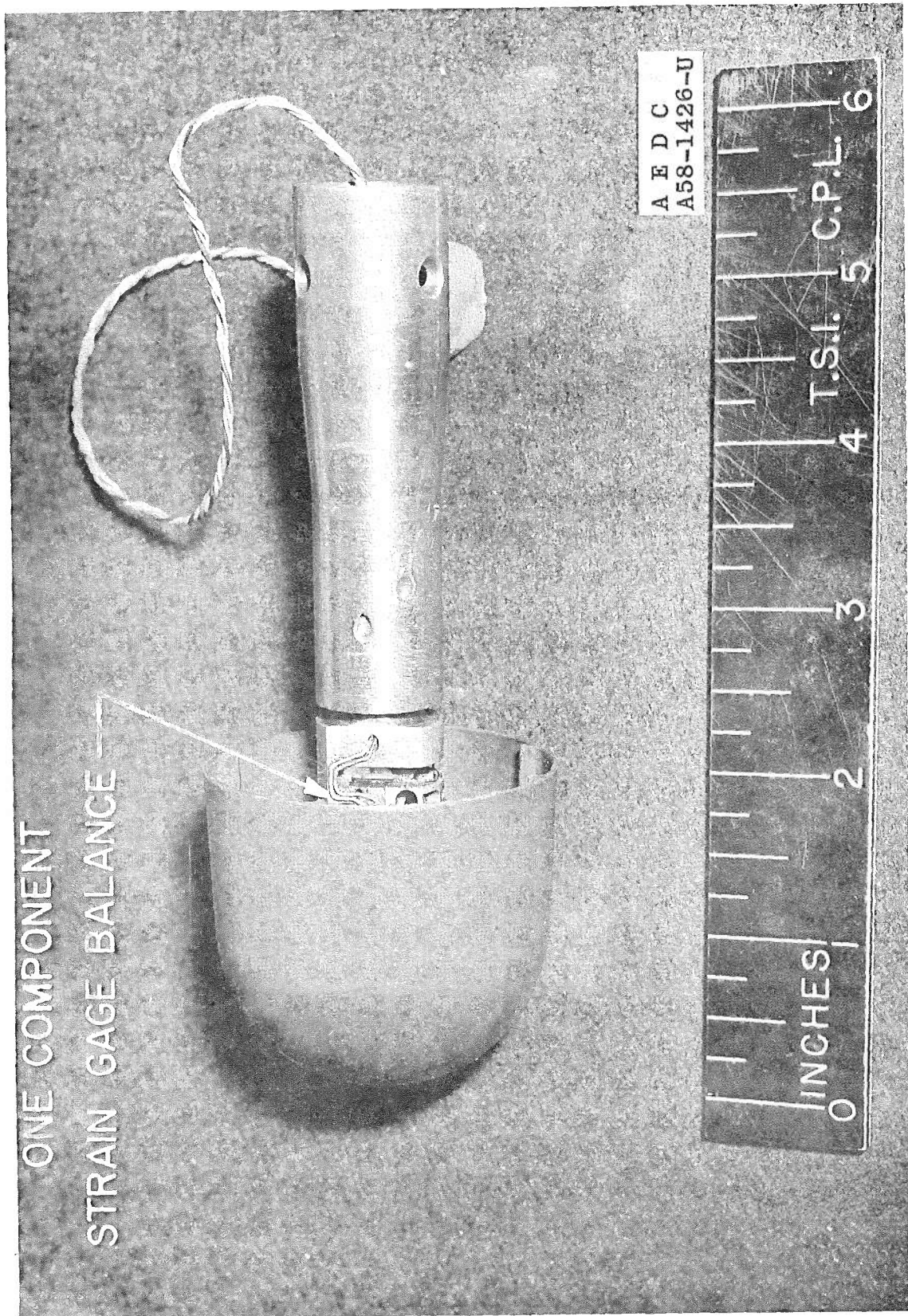


Fig. 11. Hemisphere-Cylinder Drag Model (Photo)



Fig. 12. Schlieren Photograph of Hemisphere-Cylinder

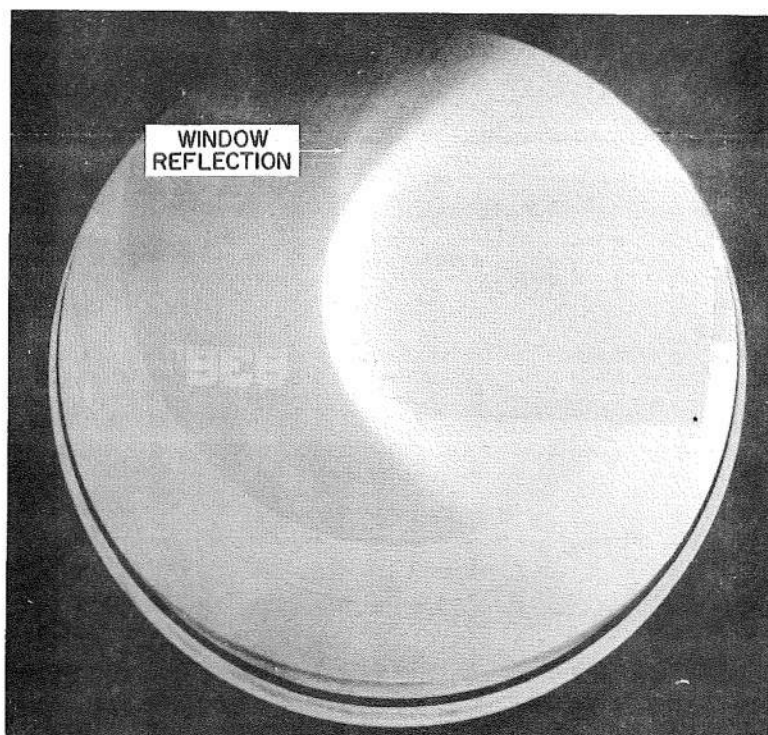


Fig. 13. Luminosity Photograph of Hemisphere-Cylinder

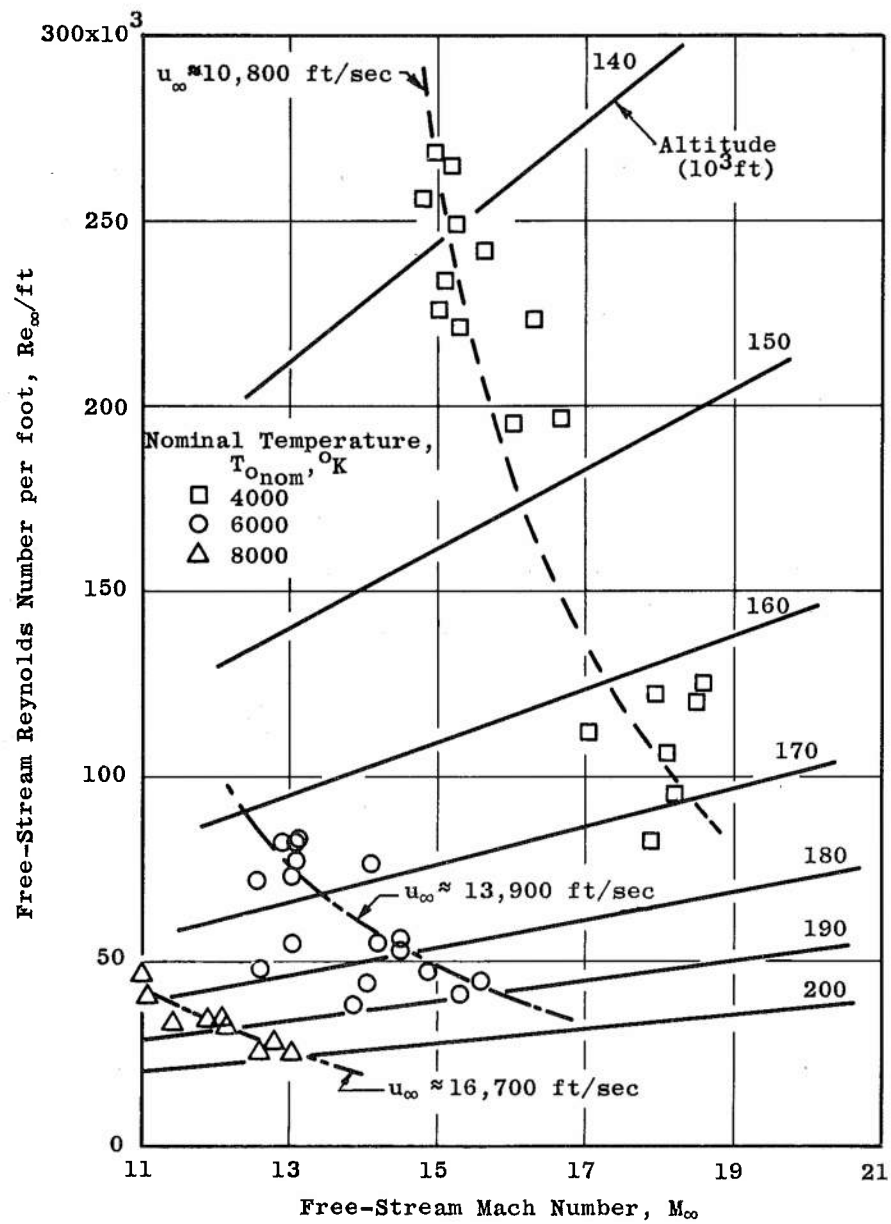


Fig. 14. Reynolds Number per Foot - Mach Number Range

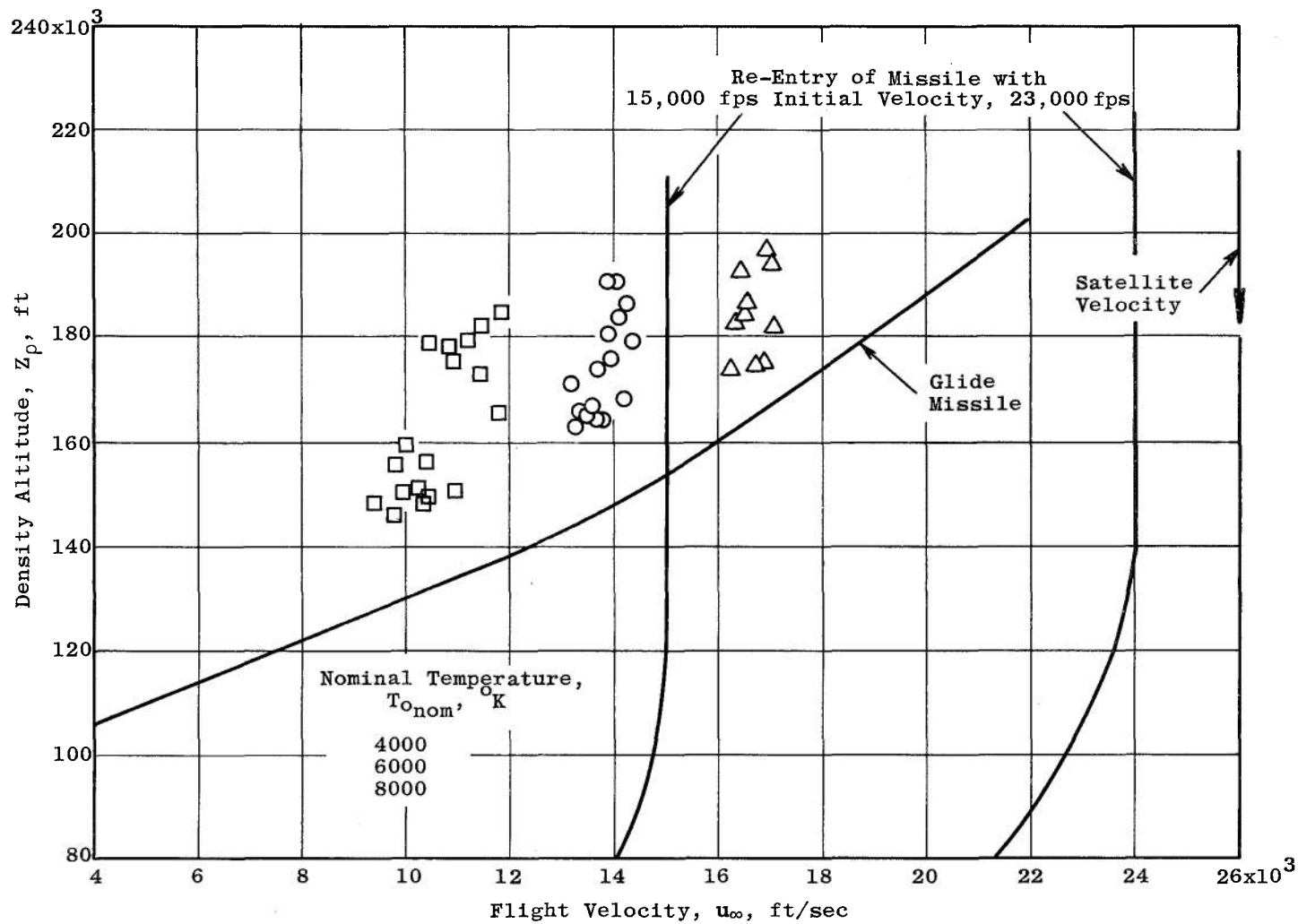


Fig. 15. Density Altitude - Velocity Comparison

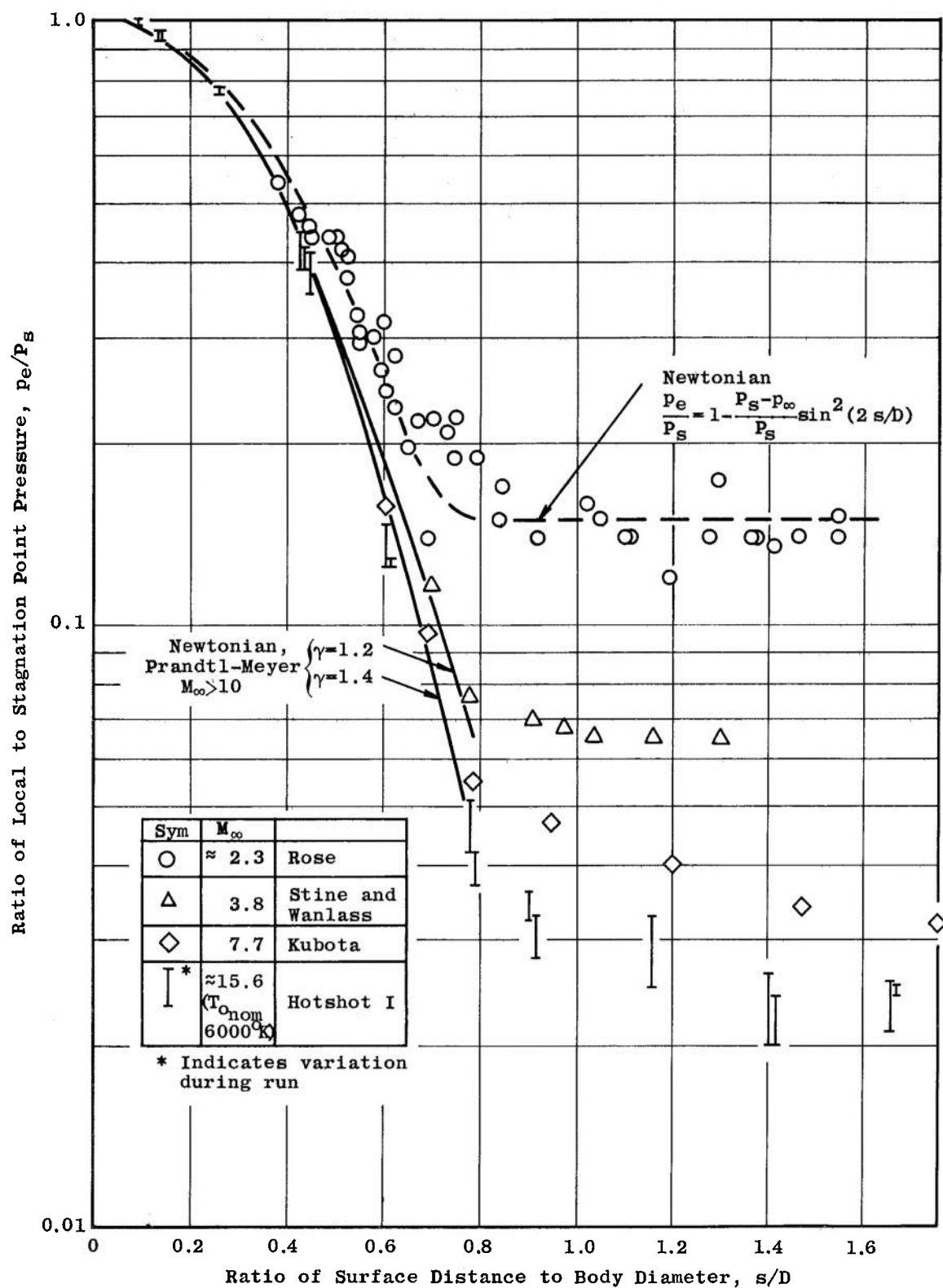


Fig. 16. Hemisphere-Cylinder Pressure Distribution, Comparison of Theory and Experiment

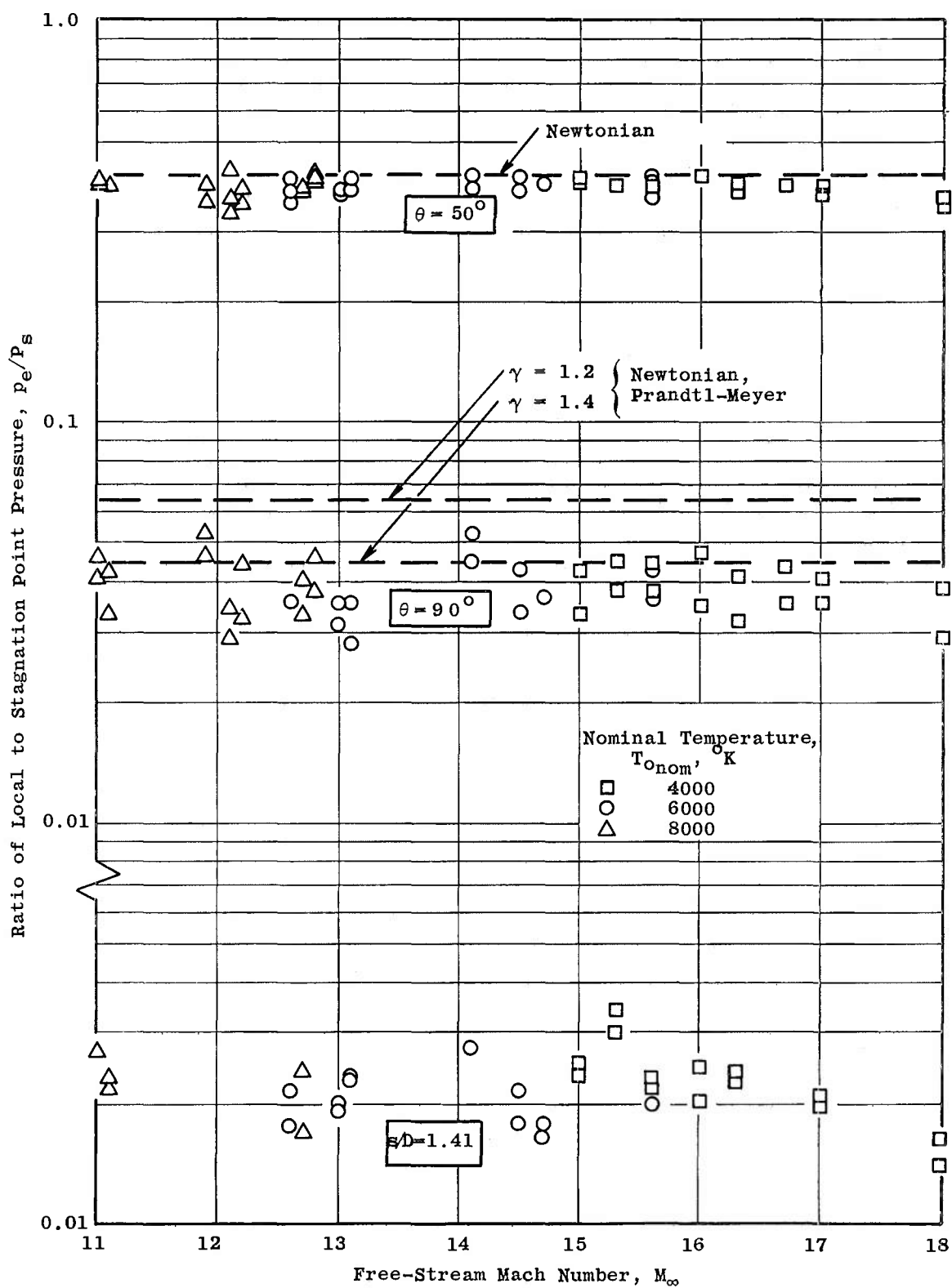


Fig. 17. Comparison of Pressure Distribution with Theory for a Hemisphere-Cylinder in Hotshot I

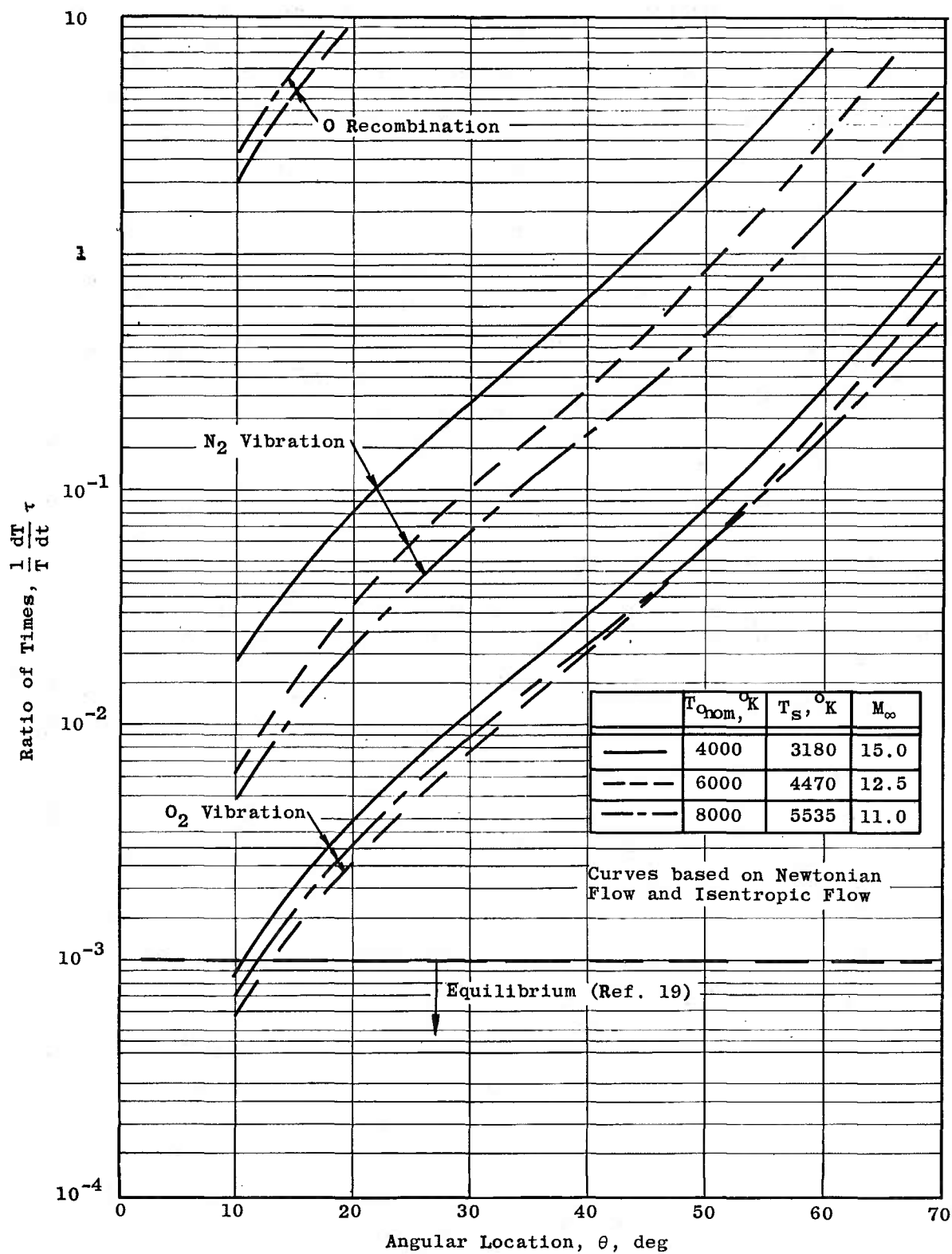


Fig. 18. Local Relaxation Characteristic Time Ratio for 2-inch Radius Hemisphere in Hotshot I

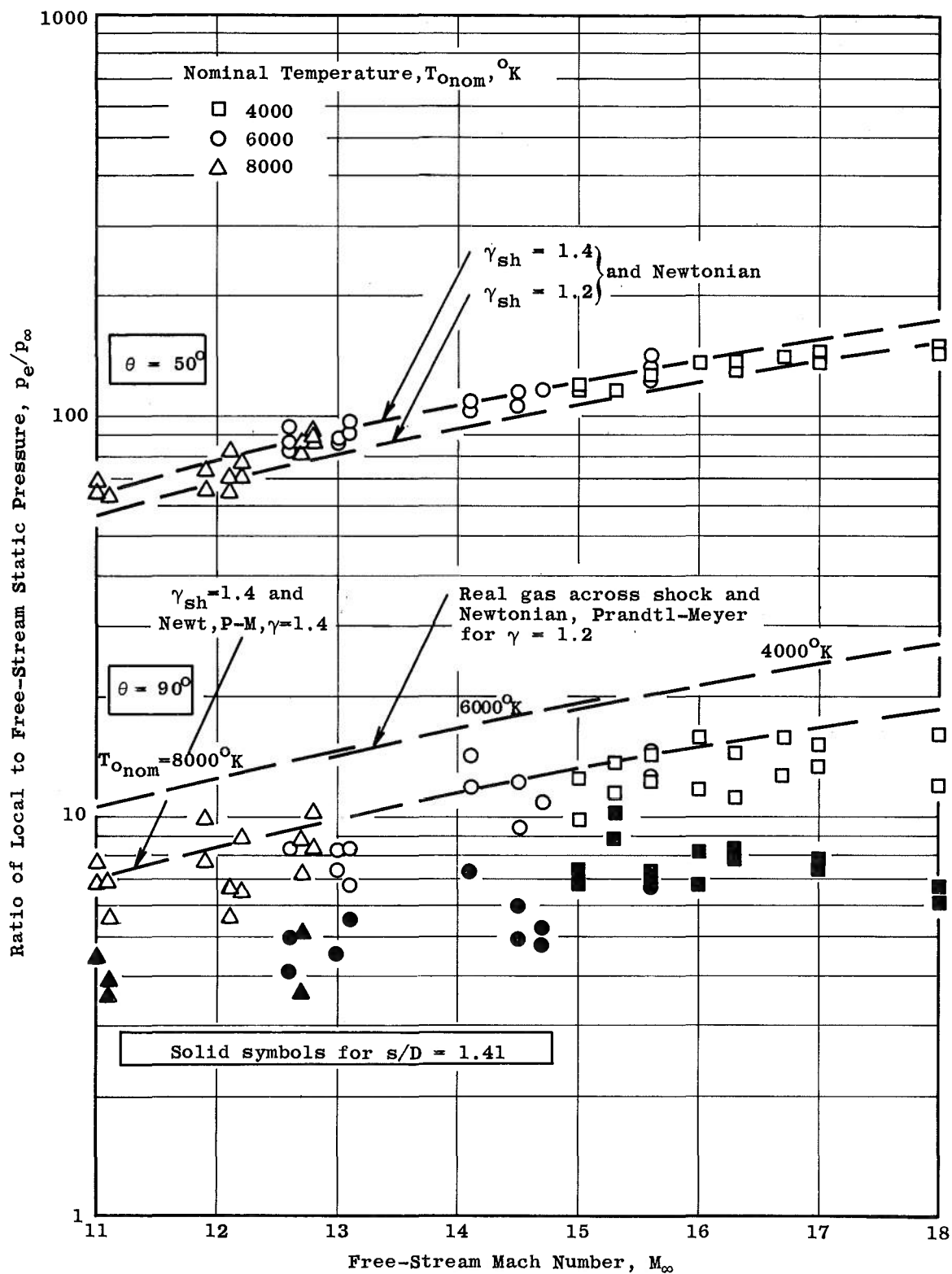


Fig. 19. Comparison of Pressure Distribution with Theory for a Hemisphere-Cylinder in Hotshot I

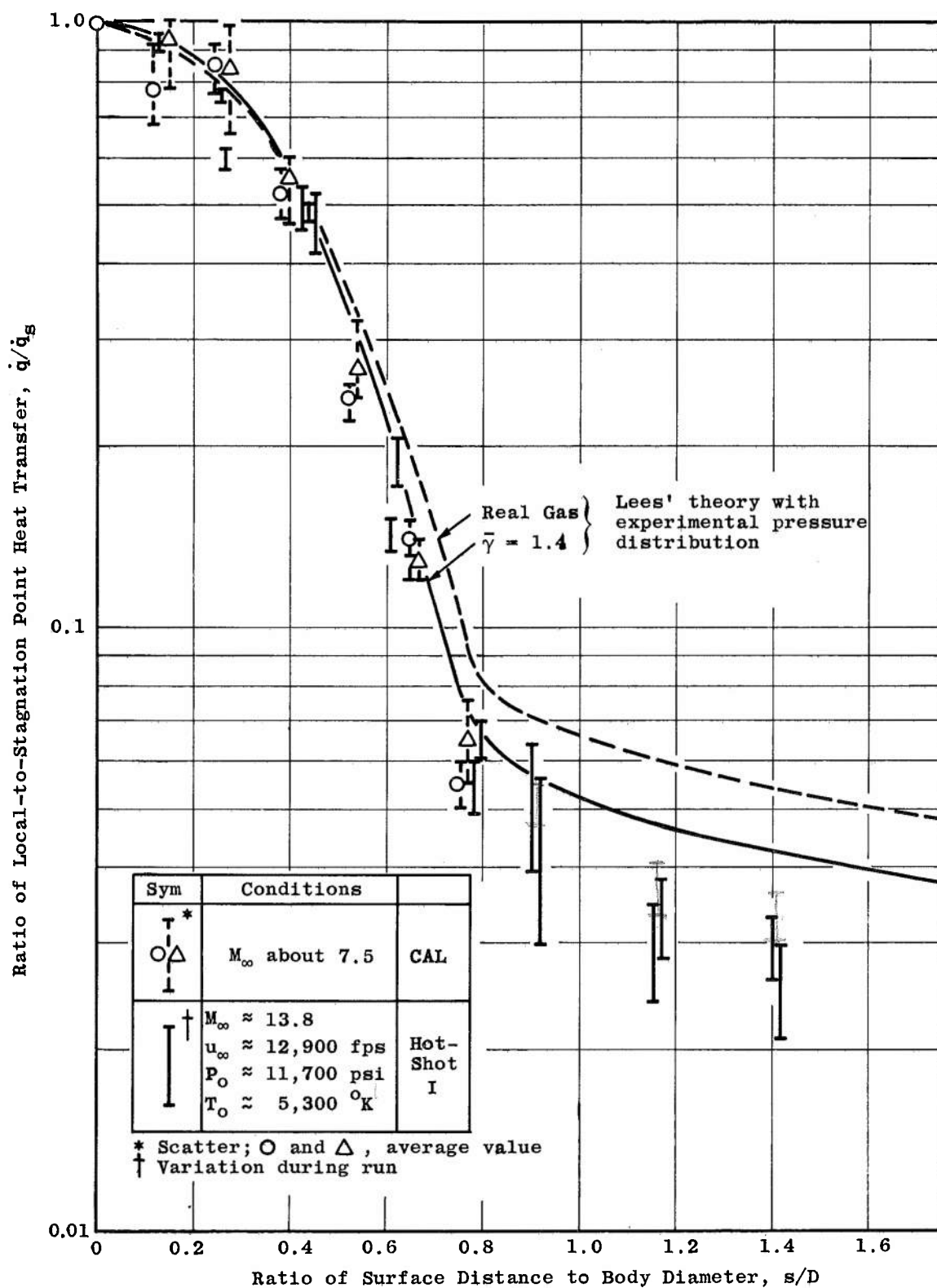


Fig. 20. Hemisphere-Cylinder Heat Transfer Distribution, Comparison of Theory and Experiment

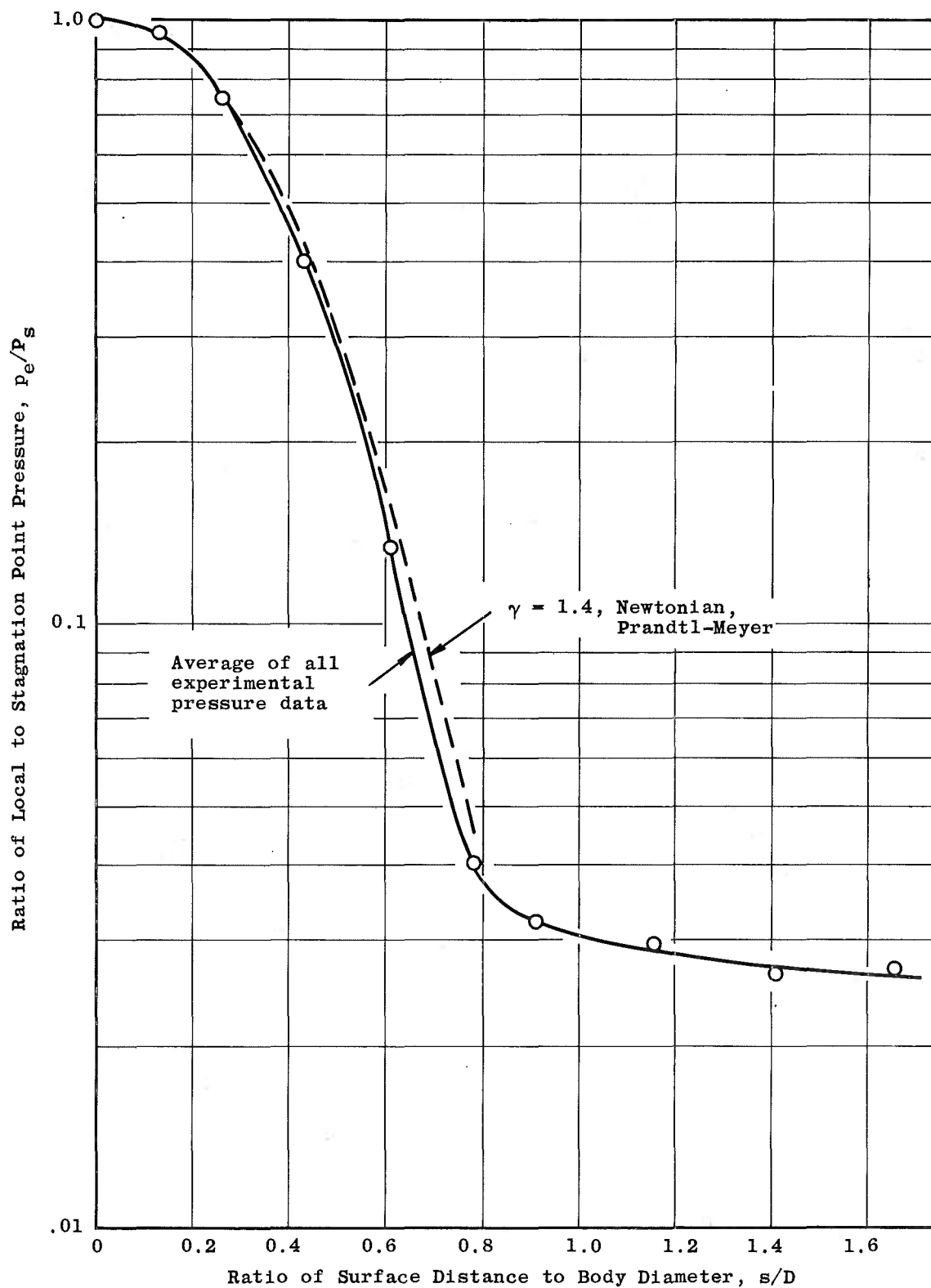


Fig. 21. Average Experimental Pressure Distribution Used for Heat Transfer Distribution Calculations for  $M_\infty > 10$

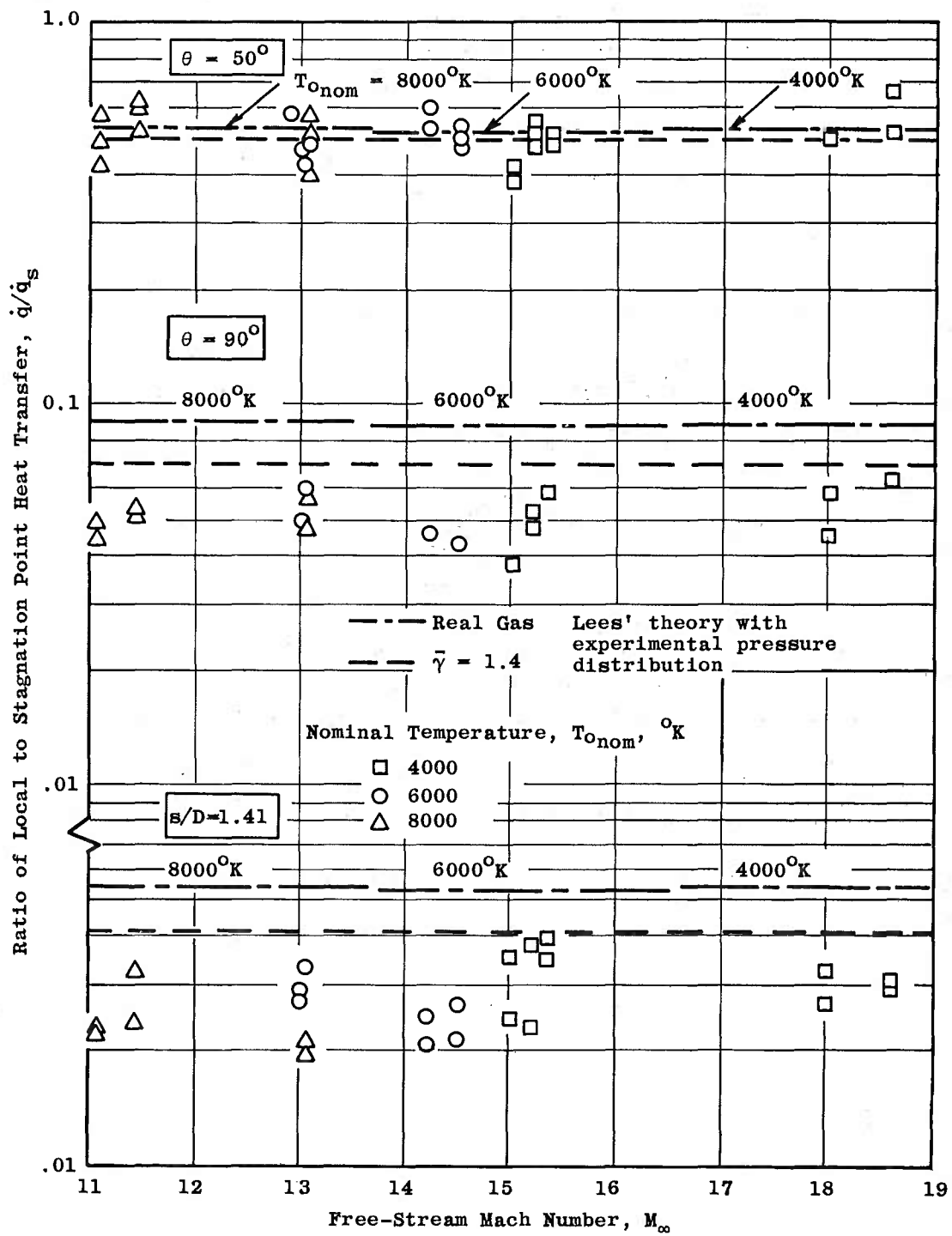


Fig. 22. Comparison of Heat Transfer Distribution with Theory for a Hemisphere-Cylinder in Hotshot I

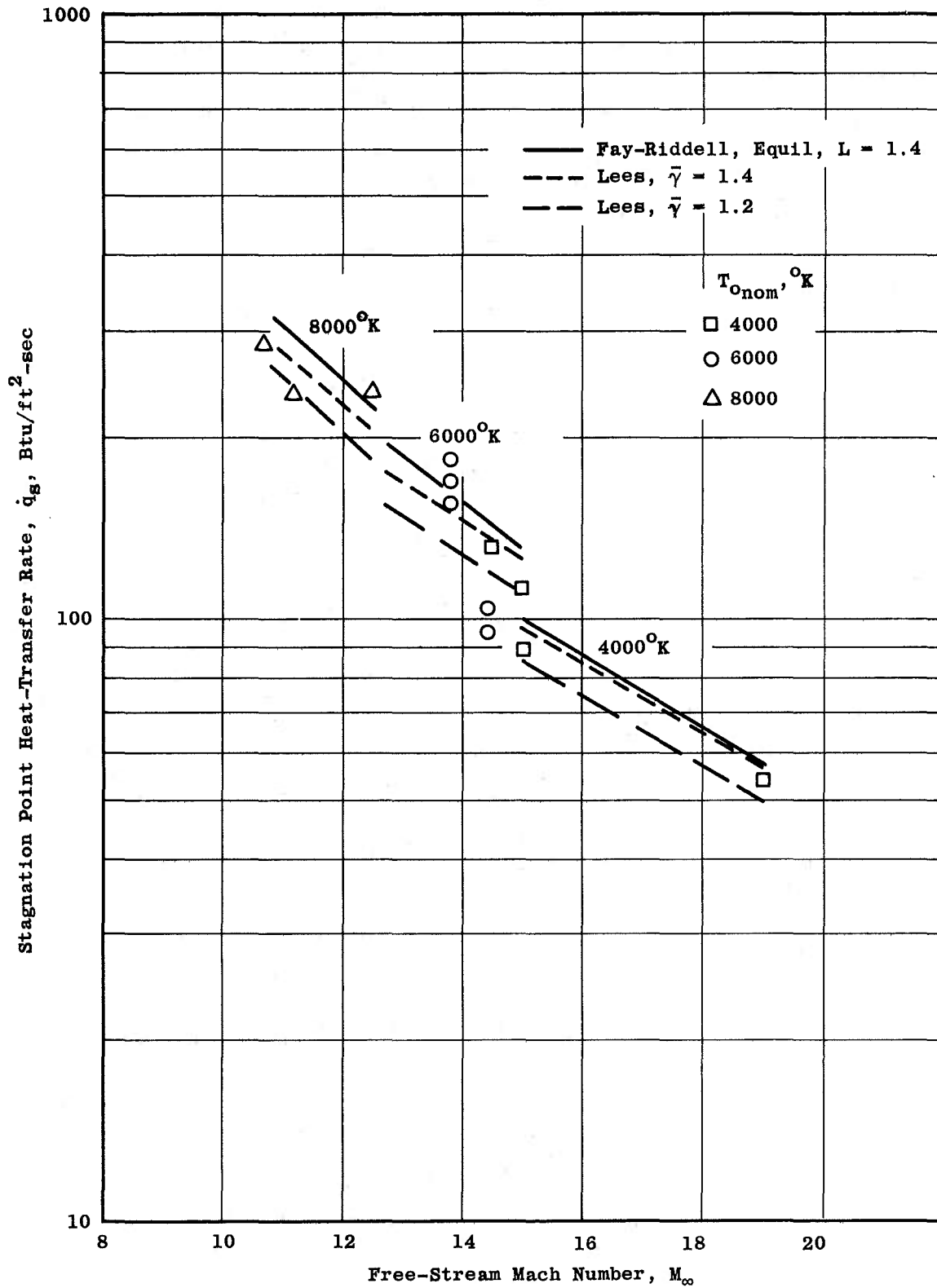


Fig. 23. Stagnation Point Heat Transfer for a Hemisphere-Cylinder in Hotshot I

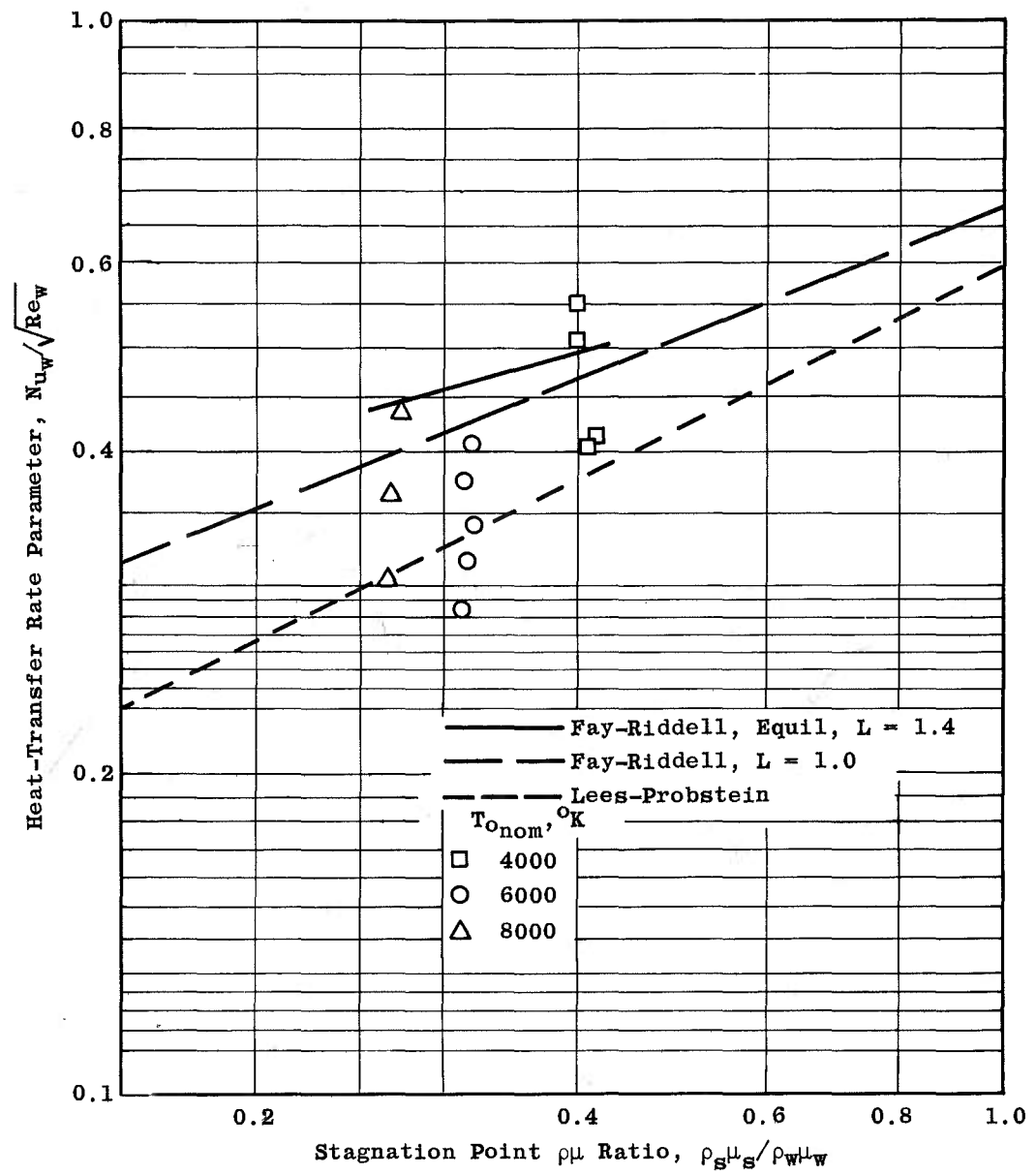


Fig. 24. Effect of  $\rho\mu$  Variation across Stagnation Point Boundary Layer

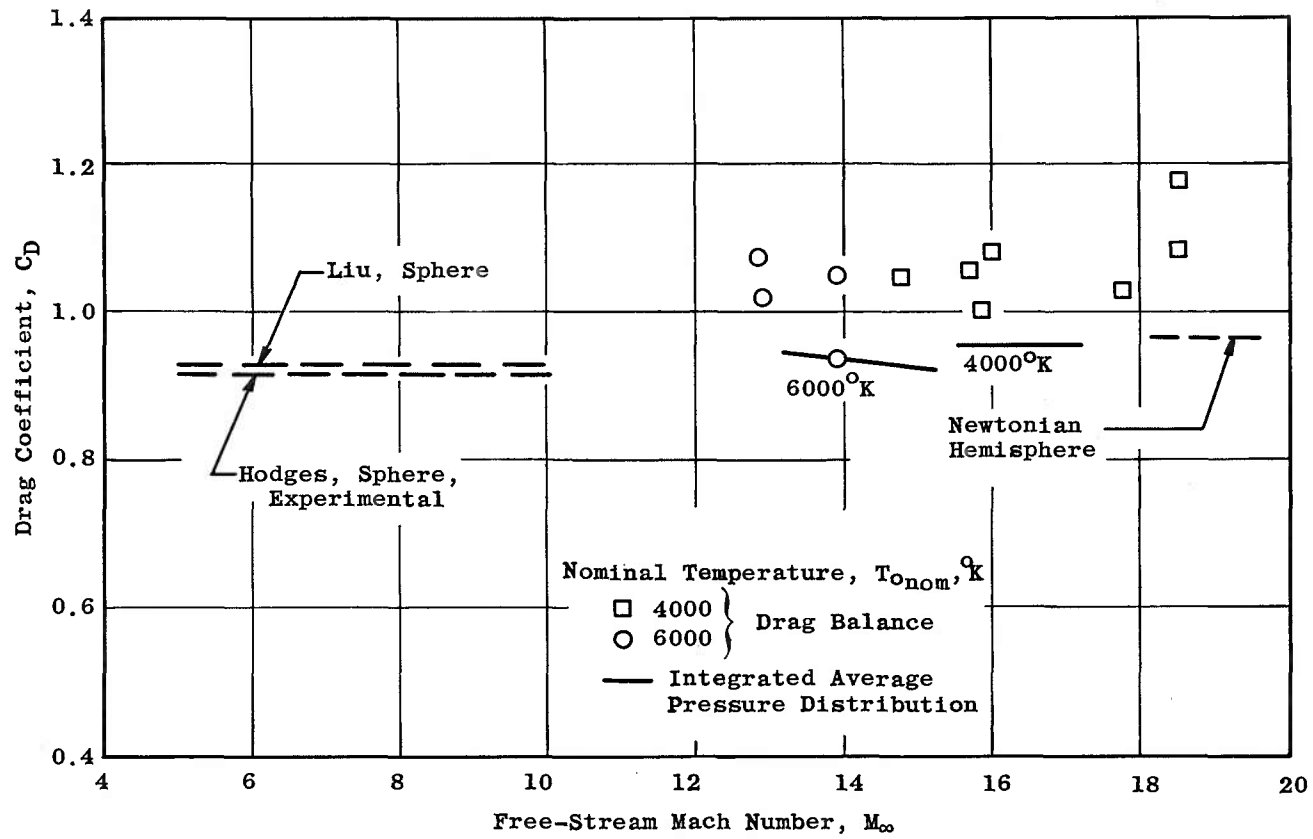


Fig. 25. Drag Coefficient for a Hemisphere-Cylinder, Comparison of Theory and Experiment

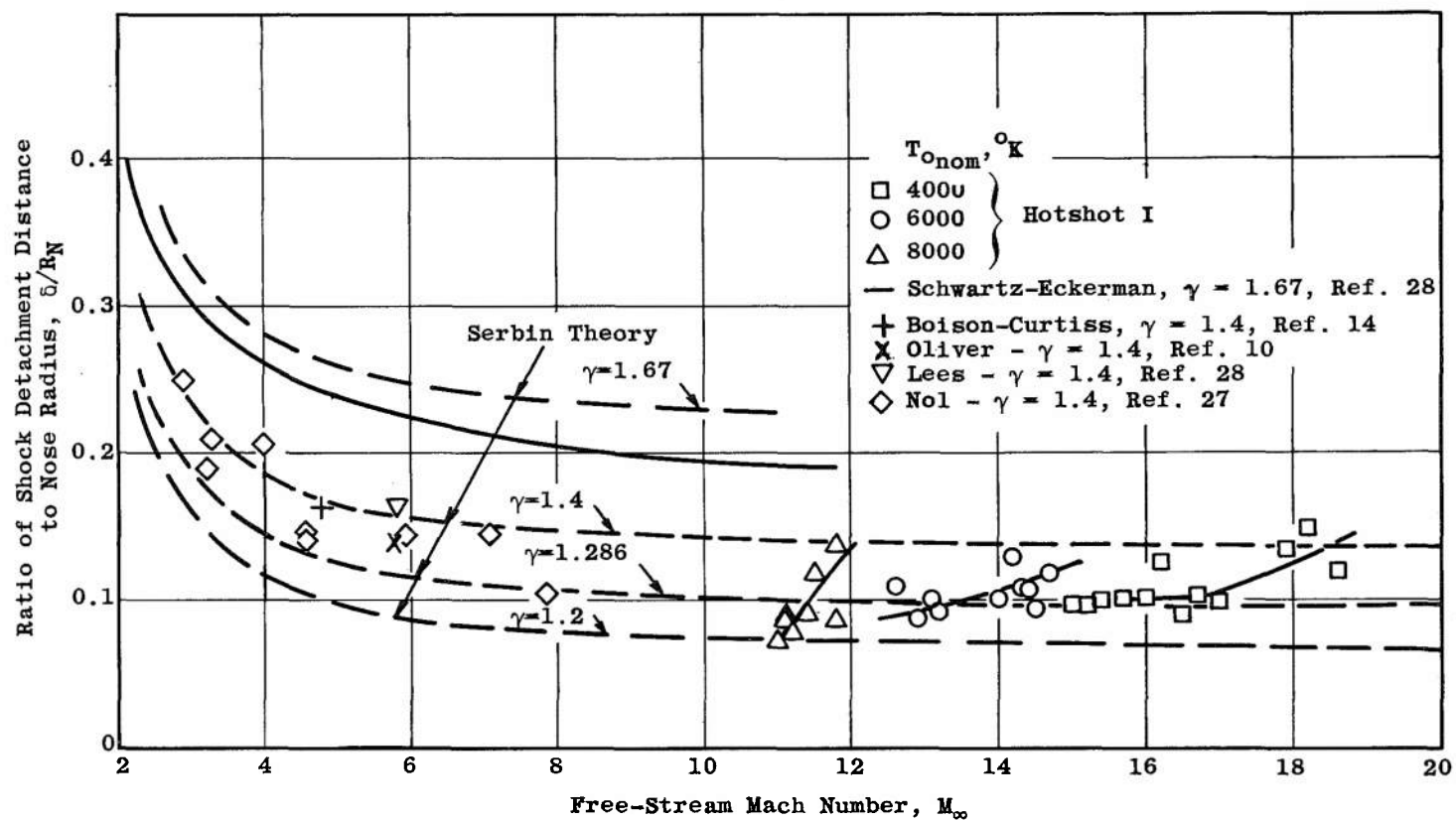


Fig. 26. Comparison of Shock Detachment Distance with Theory and Experiment